Role of sea quarks in the nucleon transverse spin

Chunhua Zeng,[1,2,3,*] Hongxin Dong,[4,†] Tianbo Liu,[5,6,‡] Peng Sun,[1,3,§] and Yuxiang Zhao[1,6,3,7,‖]

[1]*Institute of Modern Physics, Chinese Academy of Sciences, Lanzhou, Gansu 730000, China*
[2]*Lanzhou University, Lanzhou, Gansu 730000, China*
[3]*University of Chinese Academy of Sciences, Beijing 100049, China*
[4]*Department of Physics and Institute of Theoretical Physics, Nanjing Normal University, Nanjing, Jiangsu 210023, China*
[5]*Key Laboratory of Particle Physics and Particle Irradiation (MOE), Institute of Frontier and Interdisciplinary Science, Shandong University, Qingdao, Shandong 266237, China*
[6]*Southern Center for Nuclear-Science Theory (SCNT), Institute of Modern Physics, Chinese Academy of Sciences, Huizhou, Guangdong 516000, China*
[7]*Key Laboratory of Quark and Lepton Physics (MOE) and Institute of Particle Physics, Central China Normal University, Wuhan 430079, China*

(Received 8 November 2023; accepted 5 February 2024; published 4 March 2024)

We present a phenomenological extraction of transversity distribution functions and Collins fragmentation functions by simultaneously fitting to semi-inclusive deep inelastic scattering and electron-positron annihilation data. The analysis is performed within the transverse-momentum-dependent factorization formalism, and sea quark transversity distributions are taken into account for the first time. We find the $\bar{u}$ quark favors a negative transversity distribution, while that of the $\bar{d}$ quark is consistent with zero according to the current accuracy. In addition, based on a combined analysis of world data and simulated data, we quantitatively demonstrate the impact of the proposed Electron-Ion Collider in China on precise determinations of the transversity distributions, especially for sea quarks, and the Collins fragmentation functions.

DOI: 10.1103/PhysRevD.109.056002

I. INTRODUCTION

How the nucleon is built up with quarks and gluons, the fundamental degrees of freedom of quantum chromodynamics (QCD), is one of the most important questions in modern hadronic physics. Although the color confinement and nonperturbative feature of the strong interaction at hadronic scales makes it a challenging problem, the QCD factorization is established to connect quarks and gluons that participate in high-energy scatterings at subfemtometer scales and the hadrons observed by advanced detectors in experiments. In this framework, the cross section is approximated as a convolution of perturbatively calculable short-distance scattering off partons and universal long-distance functions [1,2]. Therefore, it provides an approach to extract the partonic structures of the nucleon through various experimental measurements.

The spin as a fundamental quantity of the nucleon plays an important role in unraveling its internal structures and then in understanding the properties of the strong interaction. For instance, the so-called *proton spin crisis* arose from the measurement of longitudinally polarized deep inelastic scattering (DIS) [3,4] and is still an active frontier after more than three decades. As an analog to the helicity distribution, which can be interpreted as the density of longitudinally polarized quark in a longitudinally polarized nucleon, the transversity distribution describes the net density of transversely polarized quark in a transversely polarized proton. The integral of the transversity distribution equals to the tensor charge, which characterizes the coupling to a tensor current. As the matrix element of a local tensor current operator, it has been calculated in lattice QCD with high accuracy [5–11] and is often referred to as a benchmark. In addition, a precise determination of the nucleon tensor charge will also shed light on the search of new physics beyond the standard model [12,13].

The transversity distribution has both collinear and transverse-momentum-dependent (TMD) definitions. As a chiral-odd quantity [14,15], its contribution to inclusive

*zengchunhua@impcas.ac.cn
†hxdong@nnu.edu.cn
‡liutb@sdu.edu.cn
§pengsun@impcas.ac.cn
‖yxzhao@impcas.ac.cn

DIS is highly suppressed by powers of m/Q, where m represents the quark mass and Q is the virtuality of the exchanged photon between the scattered lepton and the nucleon. A practical way to access the transversity distribution is by coupling with another chiral-odd quantity, either a fragmentation function (FF) in semi-inclusive DIS (SIDIS) process [16,17] or a distribution function in hadron-hadron collisions [18–21].

In the past two decades, many efforts have been made by HERMES [22], COMPASS [23,24], and Jefferson Lab (JLab) [25,26] via the measurement of SIDIS process on transversely polarized targets. At low transverse momentum of the produced hadron, a target transverse single spin asymmetry (SSA), named as the Collins asymmetry, can be expressed as the convolution of the transversity distribution and the Collins FF within the TMD factorization. The Collins FF, which describes a transversely polarized quark fragmenting to an unpolarized hadron, also leads to an azimuthal asymmetry in semi-inclusive e^+e^- annihilation (SIA) process, and such asymmetry has been measured by the BELLE [27], *BABAR* [28,29], and BESIII [30] Collaborations. Therefore, the transversity distribution as well as the tensor charge can be determined through a simultaneous analysis of the Collins asymmetries in SIDIS and SIA processes. We note that one can alternatively work in the collinear factorization to extract the transversity distribution via dihadron productions [31–35].

Restricted in the TMD framework, many global analyses were performed in recent years to extract the transversity distribution with or without the TMD evolution effect [36–43]. Since quark transversity distributions do not mix with gluons in the evolution, the sea quark transversity distributions were usually assumed to be zero, though some exploration to include antiquark contributions was attempted without TMD evolution [43]. This assumption might be reasonable in the exploration era, but it should eventually be tested by experiments, especially when high-precision data become available at future facilities.

After the COMPASS data taking with a transversely polarized deuteron target in the 2022–2023 run, the next generation of high-precision measurements will be the multihall SIDIS programs at the 12-GeV upgraded JLab and future electron-ion colliders. The JLab experiments will mainly cover the large-x region with relatively low Q^2. The Electron-Ion Collider (EIC) to be built at the Brookhaven National Laboratory (BNL) [44,45] will provide moderate- and large-x coverage with high Q^2. Meanwhile, it can also reach small-x values down to about 10^{-4}. The Electron-Ion Collider in China (EicC) [46] is proposed to deliver a 3.5 GeV polarized electron beam colliding with a 20 GeV polarized proton beam or a 40 GeV polarized ^{3}He beam, as well as a series of unpolarized ion beams, with designed instantaneous luminosity at about 2×10^{33} cm^{-2} s^{-1}. Its kinematic coverage will be complementary to the experiments at JLab and the EIC at BNL.

In this paper, we perform a global analysis of the Collins asymmetries in SIDIS and SIA measurement within the TMD factorization to extract the transversity distribution functions and the Collins fragmentation functions. As will be shown, there is a hint of negative $\bar{u}$ transversity distribution with about 2 standard deviations away from zero, while the $\bar{d}$ transversity distribution is consistent with zero according to the current accuracy from existing world data. Furthermore, we quantitatively study potential improvement of the EicC, which was claimed to have significant impact on the measurement of sea quark distributions. The remaining paper is organized as follows. In Sec. II, we briefly summarize the theoretical framework for the extraction of transversity distribution functions and Collins FFs from SIDIS and SIA data, leaving some detailed formulas in the appendixes. In Sec. III, we present the global analysis of world data, followed by an impact study of the EicC projected pseudodata in Sec. IV. A summary is provided in Sec. V.

II. THEORETICAL FORMALISM

In this section, the asymmetries originated from transversity TMDs and Collins FFs in SIDIS and SIA processes will be briefly reviewed, including the TMD evolution formalism to be adopted in the analysis.

A. Collins asymmetry in SIDIS

The SIDIS process is

$$e(l) + N(P) \to e(l') + h(P_h) + X, \tag{1}$$

where e denotes the incoming and outgoing lepton, N is the nucleon, and h is the detected final-state hadron. The four-momenta are given in the parentheses. Some commonly used kinematic variables are defined as

$$x = \frac{Q^2}{2P\cdot q}, \qquad y = \frac{P\cdot q}{P\cdot l}, \qquad z = \frac{P\cdot P_h}{P\cdot q}, \qquad \gamma = \frac{2xM}{Q}, \tag{2}$$

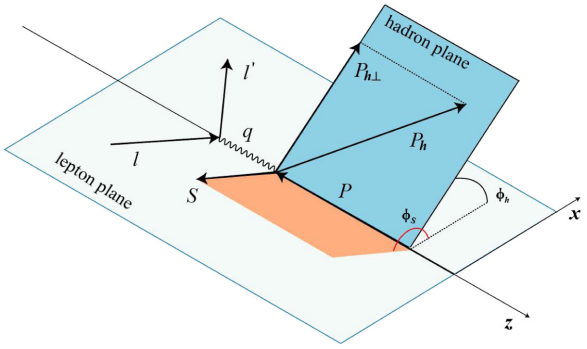

FIG. 1. The Trento convention for the definition of SIDIS kinematic variables.

where $Q^2 = -q^2 = -(l - l')^2$ is the transferred four-momentum square and M is the nucleon mass. Taking the one-photon exchange approximation, we adopt the virtual photon-nucleon frame, as illustrated in Fig. 1, and for convenience introduce the transverse metric

$$g_\perp^{\mu\nu} = g^{\mu\nu} - \frac{q^\mu P^\nu + P^\mu q^\nu}{P\cdot q(1+\gamma^2)} + \frac{\gamma^2}{1+\gamma^2}\left(\frac{q^\mu q^\nu}{Q^2} - \frac{P^\mu P^\nu}{M^2}\right) \tag{3}$$

and the transverse antisymmetric tensor

$$\epsilon_\perp^{\mu\nu} = \epsilon^{\mu\nu\rho\sigma}\frac{P_\rho q_\sigma}{P\cdot q\sqrt{1+\gamma^2}}, \tag{4}$$

with the convention $\epsilon^{0123} = 1$. Then the transverse momentum $P_{h\perp}$ and $l_\perp$ and azimuthal angles ϕ_h and the ϕ_S can be expressed in Lorentz invariant forms as

$$P_{h\perp} = \sqrt{-g_\perp^{\mu\nu}P_{h\mu}P_{h\nu}}, \tag{5}$$

$$l_\perp = \sqrt{-g_\perp^{\mu\nu}l_\mu l_\nu}, \tag{6}$$

$$\cos\phi_h = -\frac{l_\mu P_{h\nu} g_\perp^{\mu\nu}}{l_\perp P_{h\perp}}, \qquad \sin\phi_h = -\frac{l_\mu P_{h\nu}\epsilon_\perp^{\mu\nu}}{l_\perp P_{h\perp}}, \tag{7}$$

$$\cos\phi_S = -\frac{l_\mu S_{\perp\nu} g_\perp^{\mu\nu}}{l_\perp S_\perp}, \qquad \sin\phi_S = -\frac{l_\mu S_{\perp\nu}\epsilon_\perp^{\mu\nu}}{l_\perp S_\perp}, \tag{8}$$

where are known as the Trento conventions [47].

The differential cross section can be written as

$$\begin{aligned}\frac{d\sigma}{dxdydzd\phi_h d\phi_s dP_{h\perp}^2} = \frac{\alpha^2}{xyQ^2}\frac{y^2}{2(1-\epsilon)}\left(1+\frac{\gamma^2}{2x}\right)\Big\{&F_{UU,T} + \epsilon F_{UU,L} + \sqrt{2\epsilon(1+\epsilon)}\cos(\phi_h)F_{UU}^{\cos\phi_h} \\ &+ \epsilon\cos(2\phi_h)F_{UU}^{\cos 2\phi_h} + \lambda_e\sqrt{2\epsilon(1-\epsilon)}\sin(\phi_h)F_{LU}^{\sin\phi_h} + S_{||}\Big[\sqrt{2\epsilon(1+\epsilon)}\sin(\phi_h)F_{UL}^{\sin\phi_h} \\ &+ \epsilon\sin(2\phi_h)F_{UL}^{\sin 2\phi_h}\Big] + S_{||}\lambda_e\Big[\sqrt{1-\epsilon^2}F_{LL} + \sqrt{2\epsilon(1-\epsilon)}\cos(\phi_h)F_{LL}^{\cos\phi_h}\Big] \\ &+ |S_\perp|[\sin(\phi_h-\phi_s)(F_{UT,T}^{\sin(\phi_h-\phi_s)} + \epsilon F_{UT,L}^{\sin(\phi_h-\phi_s)}) + \epsilon\sin(\phi_h+\phi_s)F_{UT}^{\sin(\phi_h+\phi_s)} \\ &+ \epsilon\sin(3\phi_h-\phi_s)F_{UT}^{\sin(3\phi_h-\phi_s)} + \sqrt{2\epsilon(1+\epsilon)}\sin(\phi_s)F_{UT}^{\phi_s} + \sqrt{2\epsilon(1+\epsilon)}\sin(2\phi_h-\phi_s)F_{UT}^{\sin(2\phi_h-\phi_s)}] \\ &+ |S_\perp|\lambda_e\Big[\sqrt{1-\epsilon^2}\cos(\phi_h-\phi_s)F_{LT}^{\cos(\phi_h-\phi_s)} + \sqrt{2\epsilon(1-\epsilon)}\cos(\phi_s)F_{LT}^{\cos\phi_s} \\ &+ \sqrt{2\epsilon(1-\epsilon)}\cos(2\phi_h-\phi_s)F_{LT}^{\cos(2\phi_h-\phi_s)}\Big]\Big\},\end{aligned} \tag{9}$$

where α is the electromagnetic fine structure constant, λ_e is the lepton helicity, $S_{||(\perp)}$ is the nucleon polarization, and the structure functions F are corresponded to different azimuthal modulations indicated by the superscripts and polarization configurations indicated by the subscripts. The third subscript appearing in some terms represents the polarization of the virtual photon, and the ratio of the longitudinal and the transverse photon flux is given by

$$\epsilon = \frac{1 - y - \frac{1}{4}\gamma^2 y^2}{1 - y + \frac{1}{2}y^2 + \frac{1}{4}\gamma^2 y^2}. \tag{10}$$

For an unpolarized lepton beam scattered from a transversely polarized nucleon, the SSA can be measured by flipping the transverse polarization of the nucleon as

$$A_{UT} = \frac{1}{|S_\perp|}\frac{d\sigma(\phi_h,\phi_s) - d\sigma(\phi_h,\phi_s+\pi)}{d\sigma(\phi_h,\phi_s) + d\sigma(\phi_h,\phi_s+\pi)} = \frac{\sigma_{UT}^-}{\sigma_{UT}^+}, \tag{11}$$

where

$$\begin{aligned}\sigma_{UT}^+ = {}& F_{UU,T} + \epsilon F_{UU,L} + \sqrt{2\epsilon(1+\epsilon)}\cos(\phi_h)F_{UU}^{\cos\phi_h} \\ &+ \epsilon\cos(2\phi_h)F_{UU}^{\cos 2\phi_h},\end{aligned} \tag{12}$$

$$\begin{aligned}\sigma_{UT}^- = {}& \sin(\phi_h-\phi_s)(F_{UT,T}^{\sin(\phi_h-\phi_s)} + \epsilon F_{UT,L}^{\sin(\phi_h-\phi_s)}) \\ &+ \epsilon\sin(\phi_h+\phi_s)F_{UT}^{\sin(\phi_h+\phi_s)} \\ &+ \epsilon\sin(3\phi_h-\phi_s)F_{UT}^{\sin(3\phi_h-\phi_s)} \\ &+ \sqrt{2\epsilon(1+\epsilon)}\sin(\phi_s)F_{UT}^{\phi_s} \\ &+ \sqrt{2\epsilon(1+\epsilon)}\sin(2\phi_h-\phi_s)F_{UT}^{\sin(2\phi_h-\phi_s)}.\end{aligned} \tag{13}$$

After separating different azimuthal modulations, one can extract the Collins asymmetry as

$$\epsilon A_{UT}^{\sin(\phi_h+\phi_s)} = \frac{2\int d\phi_S d\phi_h \sin(\phi_h+\phi_S)\sigma_{UT}^-}{\int d\phi_S d\phi_h \sigma_{UT}^+} = \frac{\epsilon F_{UT}^{\sin(\phi_h+\phi_s)}}{F_{UU,T}+\epsilon F_{UU,L}}. \tag{14}$$

In this work, we neglect the term $F_{UU,L}$ and, thus,

$$A_{UT}^{\sin(\phi_h+\phi_s)} = \frac{F_{UT}^{\sin(\phi_h+\phi_s)}}{F_{UU,T}}. \tag{15}$$

To implement the TMD evolution, we perform the transverse Fourier transform, and the $P_{h\perp}$-dependent structure functions can be expressed in terms of distribution and fragmentation functions in b space as

$$F_{UU,T} = \mathcal{C}[f_1 D_1] = x\sum_q \frac{e_q^2}{2\pi}\int_0^\infty bJ_0(bP_{h\perp}/z) f_{1,q\leftarrow N}(x,b) \times D_{1,q\to h}(z,b)db, \tag{16}$$

$$F_{UT}^{\sin(\phi_h+\phi_S)} = \mathcal{C}\left[\frac{\hat{\boldsymbol{h}}\cdot\boldsymbol{p}_T}{zM_h} h_1 H_1^\perp\right] = x\sum_q \frac{M_h e_q^2}{2\pi}\int_0^\infty b^2 J_1(bP_{h\perp}/z) h_{1,q\leftarrow N}(x,b) \times H_{1,q\to h}^\perp(z,b)db, \tag{17}$$

where f_1 is the unpolarized distribution function, D_1 is the unpolarized FF, h_1 is the transversity distribution, and $H_1^\perp$ is the Collins FF, with q running over all active quark flavors: u, d, s, $\bar{u}$, $\bar{d}$, and $\bar{s}$, and e_q being the charge. The transverse momentum convolution, denoted by $\mathcal{C}[\cdots]$, is defined as

$$\mathcal{C}[wfD] = x\sum_q e_q^2 \int d^2\boldsymbol{p}_T d^2\boldsymbol{k}_\perp \delta^{(2)}(\boldsymbol{p}_T + z\boldsymbol{k}_\perp - \boldsymbol{P}_{h\perp}) \times w(\boldsymbol{p}_T,\boldsymbol{k}_\perp) f_{q\leftarrow N}(x,k_\perp) D_{q\to h}(z,p_T). \tag{18}$$

Here b is the Fourier conjugate variable to the transverse momentum of parton, $\boldsymbol{k}_\perp$ is the transverse momentum of the quark inside the nucleon, $\boldsymbol{p}_T$ is the transverse momentum of the final-state hadron with respect to the parent quark momentum, and $\hat{\boldsymbol{h}} = \boldsymbol{P}_{h\perp}/|\boldsymbol{P}_{h\perp}|$ represents the transverse direction of the final-state hadron. More details of these expressions are given in Appendixes B and C.

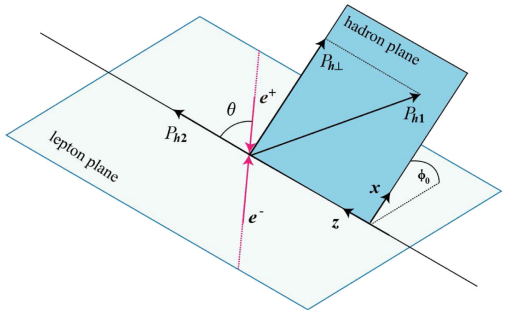

FIG. 2. The reference frame for the SIA process.

B. Collins asymmetries in SIA

Considering the SIA process

$$e^+(l_{e^+}) + e^-(l_{e^-}) \to h_1(P_{h1}) + h_2(P_{h2}) + X, \tag{19}$$

one can introduce the variables $z_i = 2P_{hi}\cdot q/Q$ $(i = 1, 2)$ with $q = l_{e^+} + l_{e^-}$ and $Q^2 = q^2$. With one-photon exchange approximation, the differential cross section can be expressed in terms of the structure functions $F_{uu}^{h_1h_2}$ and $F_{\text{Collins}}^{h_1h_2}$ as

$$\frac{d^5\sigma}{dz_1dz_2d^2\boldsymbol{P}_{h\perp}d\cos\theta} = \frac{3\pi\alpha^2}{2Q^2} z_1^2 z_2^2 [(1+\cos^2\theta)F_{uu}^{h_1h_2} + \sin^2\theta\cos(2\phi_0)F_{\text{Collins}}^{h_1h_2}]. \tag{20}$$

As illustrated in Fig. 2, θ is the polar angle between the hadron h_2 and the beam of e^+e^-, ϕ_0 is the azimuthal angle from the lepton plane to the hadron plane, and $P_{h\perp}$ is the transverse momentum of hadron h_1.

When the two hadrons are nearly back to back, where the TMD factorization is appropriate, one can express the structure functions $F_{uu}^{h_1h_2}$ and $F_{\text{Collins}}^{h_1h_2}$ in terms of TMD FFs as

$$F_{uu}^{h_1h_2} = \mathcal{C}[D_1D_1] = \frac{1}{2\pi}\sum_q e_q^2 \int J_0(P_{h\perp}b/z_1) \times D_{1,q\to h_1}(z_1,b) D_{1,\bar{q}\to h_2}(z_2,b)bdb, \tag{21}$$

$$F_{\text{Collins}}^{h_1h_2} = \mathcal{C}\left[\frac{2(\hat{\boldsymbol{h}}\cdot\boldsymbol{p}_{1T})(\hat{\boldsymbol{h}}\cdot\boldsymbol{p}_{2T}) - \boldsymbol{p}_{1T}\cdot\boldsymbol{p}_{2T}}{z_1z_2M_{h_1}M_{h_2}} H_1^\perp H_1^\perp\right] = \frac{M_{h_1}M_{h_2}}{2\pi}\sum_q e_q^2 \int J_2(P_{h\perp}b/z_1) \times H_{1,q\to h_1}^\perp(z_1,b) H_{1,\bar{q}\to h_2}^\perp(z_2,b) b^3db, \tag{22}$$

where the transverse momentum convolution $\mathcal{C}[\cdots]$ is defined as

$$\mathcal{C}[wDD] = \sum_q e_q^2 \int \frac{d^2\boldsymbol{p}_{1T}}{z_1^2}\frac{d^2\boldsymbol{p}_{2T}}{z_2^2}\delta^{(2)}\left(-\frac{\boldsymbol{p}_{1T}}{z_1}-\frac{\boldsymbol{p}_{2T}}{z_2}+\frac{\boldsymbol{P}_{h\perp}}{z_1}\right) \times w(\boldsymbol{p}_{1T},\boldsymbol{p}_{2T})D_{q\to h_1}(z_1,p_{1T})D_{\bar{q}\to h_2}(z_2,p_{2T}). \tag{23}$$

More details are provided in Appendix C.

In order to extract Collins effect corresponding to the $\cos 2\phi_0$ azimuthal dependence, one can rewritten the differential cross section (20) as

$$\frac{d^5\sigma}{dz_1 dz_2 d^2\boldsymbol{P}_{h\perp} d\cos\theta} = \frac{3\pi\alpha^2 z_1^2 z_2^2}{2Q^2}(1+\cos^2\theta)F_{uu}^{h_1h_2}R^{h_1h_2}, \tag{24}$$

where

$$R^{h_1h_2}(z_1,z_2,\theta,P_{h\perp}) = 1+\cos(2\phi_0)\frac{\sin^2\theta}{1+\cos^2\theta}\frac{F_{\text{Collins}}^{h_1h_2}}{F_{uu}^{h_1h_2}}. \tag{25}$$

The $P_{h\perp}$-integrated modulation can be accordingly defined as

$$R^{h_1h_2}(z_1,z_2,\theta) = 1+\cos(2\phi_0)\frac{\sin^2\theta}{1+\cos^2\theta}\frac{\int dP_{h\perp}P_{h\perp}F_{\text{Collins}}^{h_1h_2}}{\int dP_{h\perp}P_{h\perp}F_{uu}^{h_1h_2}}. \tag{26}$$

To reduce the systematic uncertainty caused by false asymmetry, the ratio between the hadron pair production with unlike sign, labeled by "U," and that with like sign, labeled by "L," is usually measured in experiment. Following the above formalism, it can be written as

$$\begin{aligned} R^{UL} &= \frac{R^U}{R^L} = \frac{1+\cos(2\phi_0)\frac{\langle\sin^2\theta\rangle}{\langle 1+\cos^2\theta\rangle}P_U}{1+\cos(2\phi_0)\frac{\langle\sin^2\theta\rangle}{\langle 1+\cos^2\theta\rangle}P_L} \\ &\simeq 1+\cos(2\phi_0)\frac{\langle\sin^2\theta\rangle}{\langle 1+\cos^2\theta\rangle}(P_U-P_L) \\ &= 1+\cos(2\phi_0)A_0^{UL}, \end{aligned} \tag{27}$$

where

$$P_U(z_1,z_2,P_{h\perp}) = \frac{F_{\text{Collins}}^U}{F_{uu}^U}, \tag{28}$$

$$P_L(z_1,z_2,P_{h\perp}) = \frac{F_{\text{Collins}}^L}{F_{uu}^L}, \tag{29}$$

$$P_U(z_1,z_2) = \frac{\int dP_{h\perp}P_{h\perp}F_{\text{Collins}}^U}{\int dP_{h\perp}P_{h\perp}F_{uu}^U}, \tag{30}$$

$$P_L(z_1,z_2) = \frac{\int dP_{h\perp}P_{h\perp}F_{\text{Collins}}^L}{\int dP_{h\perp}P_{h\perp}F_{uu}^L}, \tag{31}$$

and

$$A_0^{UL} = \frac{\langle\sin^2\theta\rangle}{\langle 1+\cos^2\theta\rangle}(P_U-P_L) \tag{32}$$

is referred to as the Collins asymmetry in the SIA process. For $\pi\pi$ channels, one has

$$F_{uu}^U = F_{uu}^{\pi^+\pi^-}+F_{uu}^{\pi^-\pi^+}, \tag{33}$$

$$F_{uu}^L = F_{uu}^{\pi^+\pi^+}+F_{uu}^{\pi^-\pi^-}, \tag{34}$$

$$F_{\text{Collins}}^U = F_{\text{Collins}}^{\pi^+\pi^-}+F_{\text{Collins}}^{\pi^-\pi^+}, \tag{35}$$

$$F_{\text{Collins}}^L = F_{\text{Collins}}^{\pi^+\pi^+}+F_{\text{Collins}}^{\pi^-\pi^-}; \tag{36}$$

for KK channels, one has

$$F_{uu}^U = F_{uu}^{K^+K^-}+F_{uu}^{K^-K^+}, \tag{37}$$

$$F_{uu}^L = F_{uu}^{K^+K^+}+F_{uu}^{K^-K^-}, \tag{38}$$

$$F_{\text{Collins}}^U = F_{\text{Collins}}^{K^+K^-}+F_{\text{Collins}}^{K^-K^+}, \tag{39}$$

$$F_{\text{Collins}}^L = F_{\text{Collins}}^{K^+K^+}+F_{\text{Collins}}^{K^-K^-}; \tag{40}$$

and for $K\pi$ channels, one has

$$F_{uu}^U = F_{uu}^{\pi^+K^-}+F_{uu}^{\pi^-K^+}+F_{uu}^{K^+\pi^-}+F_{uu}^{K^-\pi^+}, \tag{41}$$

$$F_{uu}^L = F_{uu}^{\pi^+K^+}+F_{uu}^{\pi^-K^-}+F_{uu}^{K^+\pi^+}+F_{uu}^{K^-\pi^-}, \tag{42}$$

$$F_{\text{Collins}}^U = F_{\text{Collins}}^{\pi^+K^-}+F_{\text{Collins}}^{\pi^-K^+}+F_{\text{Collins}}^{K^+\pi^-}+F_{\text{Collins}}^{K^-\pi^+}, \tag{43}$$

$$F_{\text{Collins}}^L = F_{\text{Collins}}^{\pi^+K^+}+F_{\text{Collins}}^{\pi^-K^-}+F_{\text{Collins}}^{K^+\pi^+}+F_{\text{Collins}}^{K^-\pi^-}. \tag{44}$$

C. TMD evolution formalism

The TMD evolution is implemented in the b space. There are two types of energy dependence in TMDs, namely, (μ,ζ), where μ is the renormalization scale related to the corresponding collinear parton distribution functions (PDFs) and FFs, and ζ serves as a cutoff scale to regularize the light-cone singularity in the operator definition of TMDs. In order to minimize the uncertainty from the scale dependence, the scales are usually set as $\mu^2=\zeta=Q^2$. Besides, for a fixed order perturbative expansion, one will find terms containing $[\alpha_s\ln^2(Qb)]^n$ and $[\alpha_s\ln(Qb)]^n$ at the nth order in powers of the strong coupling constant α_s. To ensure accurate predictions in perturbation theory, we have to resum these large logarithms of all orders into an

evolution factor $R[b;(\mu_i,\zeta_i)\to(Q,Q^2)]$, which is determined by the equations

$$\mu^2\frac{dF(x,b;\mu,\zeta)}{d\mu^2}=\frac{\gamma_F(\mu,\zeta)}{2}F(x,b;\mu,\zeta), \tag{45}$$

$$\zeta\frac{dF(x,b;\mu,\zeta)}{d\zeta}=-\mathcal{D}(b,\mu)F(x,b;\mu,\zeta), \tag{46}$$

where $\gamma_F(\mu,\zeta)$ and $\mathcal{D}(b,\mu)$ are, respectively, the TMD anomalous dimension and the rapidity anomalous dimension, and F stands for some TMD function, i.e., $f_1(x,b;\mu,\zeta)$, $h_1(x,b;\mu,\zeta)$, $D_1(z,b;\mu,\zeta)$, or $H_{1T}^{\perp}(z,b;\mu,\zeta)$ in this work. By solving the equations above, the TMD evolution can be expressed as a path integral from (μ_i,ζ_i) to (Q,Q^2) as

$$R[b;(\mu_i,\zeta_i)\to(Q,Q^2)]=\exp\left[\int_{\mathcal{P}}\left(\frac{\gamma_F(\mu,\zeta)}{\mu}d\mu-\frac{\mathcal{D}(\mu,b)}{\zeta}d\zeta\right)\right]. \tag{47}$$

Then one can formally relate the TMD functions between (Q,Q^2) and (μ_i,ζ_i) via

$$\begin{aligned}
f_1(x,b;Q,Q^2)D_1(z,b;Q,Q^2)&=R^2[b;(\mu_i,\zeta_i)\to(Q,Q^2)]f_1(x,b;\mu_i,\zeta_i)D_1(z,b;\mu_i,\zeta_i),\\
h_1(x,b;Q,Q^2)H_{1T}^{\perp}(z,b;Q,Q^2)&=R^2[b;(\mu_i,\zeta_i)\to(Q,Q^2)]h_1(x,b;\mu_i,\zeta_i)H_{1T}^{\perp}(z,b;\mu_i,\zeta_i),\\
D_1(z,b;Q,Q^2)D_1(z,b;Q,Q^2)&=R^2[b;(\mu_i,\zeta_i)\to(Q,Q^2)]D_1(z,b;\mu_i,\zeta_i)D_1(z,b;\mu_i,\zeta_i),\\
H_{1T}^{\perp}(z,b;Q,Q^2)H_{1T}^{\perp}(z,b;Q,Q^2)&=R^2[b;(\mu_i,\zeta_i)\to(Q,Q^2)]H_{1T}^{\perp}(z,b;\mu_i,\zeta_i)H_{1T}^{\perp}(z,b;\mu_i,\zeta_i).
\end{aligned} \tag{48}$$

The evolution factor R is path independent if the complete perturbative expansion is taken into account, and then one can, in principle, arbitrarily choose the path $\mathcal{P}$ in Eq. (47). However, this property is compromised when the perturbative expansion is truncated, while it is evident that the discrepancies from path to path diminish as more terms are incorporated in the perturbative expansions. The precision for the perturbative calculation of the factors in powers of α_s in evolution of this work is summarized in Table I.

In the ζ prescription [48], a special path $\mathcal{P}$ is suggested, so that Eq. (47) has a simple form:

$$R[b;(\mu_i,\zeta_i)\to(Q,Q^2)]=\left(\frac{Q^2}{\zeta_\mu(Q,b)}\right)^{-\mathcal{D}(Q,b)}, \tag{49}$$

where $\zeta_\mu(Q,b)$ is determined by solving the equation

$$\frac{d\ln\zeta_\mu(\mu,b)}{d\ln\mu^2}=\frac{\gamma_F(\mu,\zeta_\mu(\mu,b))}{2\mathcal{D}(\mu,b)} \tag{50}$$

with the boundary conditions

$$\mathcal{D}(\mu_0,b)=0,\qquad \gamma_F(\mu_0,\zeta_\mu(\mu_0,b))=0, \tag{51}$$

where $\mathcal{D}(\mu,b)$ is expressed as

TABLE I. The precision of various factors in powers of α_s for the evolution.

Evolution	$\Gamma_{\rm cusp}$	γ_V	$\mathcal{D}_{\rm resum}$	$\zeta_\mu^{\rm pert}$	$\zeta_\mu^{\rm exact}$
NNLO	α_s^3	α_s^2	α_s^2	α_s^1	α_s^1

$$\mathcal{D}(\mu,b)=\mathcal{D}_{\rm resum}(\mu,b^*)+d_{\rm NP}(b), \tag{52}$$

with $d_{\rm NP}(b)=c_0bb^*$, and $\zeta_\mu(\mu,b)$ is expressed as

$$\begin{aligned}
\zeta_\mu(\mu,b)=&\,\zeta_\mu^{\rm pert}(\mu,b)e^{-b^2/B_{\rm NP}^2}\\
&+\zeta_\mu^{\rm exact}(\mu,b)(1-e^{-b^2/B_{\rm NP}^2}).
\end{aligned} \tag{53}$$

The free parameters are set as $B_{\rm NP}=1.93\ {\rm GeV}^{-1}$ and $c_0=0.0391\ {\rm GeV}^2$ as determined in [48] by fitting unpolarized SIDIS and Drell-Yan data. More details on $\mathcal{D}(\mu,b)$ and $\zeta_\mu(\mu,b)$ can be found in Appendix A.

D. Unpolarized TMD PDFs and FFs

According to the phenomenological *Ansätze* in Ref. [48], the unpolarized TMDs and FFs can be written as

$$\begin{aligned}
f_{1,f\leftarrow h}(x,b;\mu_i,\zeta_i)=&\sum_{f'}\int_x^1\frac{dy}{y}C_{f\leftarrow f'}(y,b,\mu_{\rm OPE}^{\rm PDF})\\
&\times f_{1,f'\leftarrow h}\left(\frac{x}{y},\mu_{\rm OPE}^{\rm PDF}\right)f_{\rm NP}(x,b),\\
D_{1,f\to h}(z,b;\mu_i,\zeta_i)=&\frac{1}{z^2}\sum_{f'}\int_z^1\frac{dy}{y}y^2\mathbb{C}_{f\to f'}(y,b,\mu_{\rm OPE}^{\rm FF})\\
&\times d_{1,f'\to h}\left(\frac{z}{y},\mu_{\rm OPE}^{\rm FF}\right)D_{\rm NP}(z,b),
\end{aligned} \tag{54}$$

where $f_{\rm NP}(x,b)$ and $D_{\rm NP}(z,b)$ are nonperturbative functions, $f_{1,f'\leftarrow h}(x,\mu)$ and $d_{1,f'\to h}(z,\mu)$ are collinear PDFs and FFs, and $C_{f\leftarrow f'}(y,b,\mu)$ and $\mathbb{C}_{f\to f'}(y,b,\mu)$ are matching coefficients calculated via the operator product expansion methods [49].

The $C(\mathbb{C})$ functions are taken into account up to the one-loop order, with explicit expressions given in Appendix D. The evolution scales $\mu_{\rm OPE}^{\rm PDF}$ and $\mu_{\rm OPE}^{\rm FF}$ within the ζ prescription can be written as [48]

$$\mu_{\rm OPE}^{\rm PDF} = \frac{2e^{-\gamma_E}}{b} + 2\ \text{GeV}, \tag{55}$$

$$\mu_{\rm OPE}^{\rm FF} = \frac{2e^{-\gamma_E} z}{b} + 2\ \text{GeV}, \tag{56}$$

and the 2 GeV is a large-b offset of $\mu_{\rm OPE}$ which is a typical reference scale for PDFs and FFs. The parametrized form of the nonperturbative functions $f_{\rm NP}(x,b)$ and $D_{\rm NP}(z,b)$ can be adopted as [48]

$$f_{\rm NP}(x,b) = \exp\left[-\frac{\lambda_1(1-x)+\lambda_2 x + x(1-x)\lambda_5}{\sqrt{1+\lambda_3 x^{\lambda_4} b^2}} b^2\right], \tag{57}$$

$$D_{\rm NP}(z,b) = \exp\left[-\frac{\eta_1 z + \eta_2(1-z)}{\sqrt{1+\eta_3(b/z)^2}} \frac{b^2}{z^2}\right]\left(1+\eta_4 \frac{b^2}{z^2}\right), \tag{58}$$

TABLE II. The values of the parameters for nonperturbative functions in Eqs. (57) and (58). Their units are in GeV^2 except for λ_4, which is dimensionless.

λ_1	λ_2	λ_3	λ_4	λ_5
0.198	9.30	431	2.12	−4.44

η_1	η_2	η_3	η_4
0.260	0.476	0.478	0.483

where the parameters λ and η are extracted from the fit of unpolarized SIDIS and Drell-Yan data, specifically at low transverse momentum. Their values are listed in Table II.

III. EXTRACTION OF TRANSVERSITY DISTRIBUTIONS AND COLLINS FFs

In this section, we present the global analysis of the SIDIS and SIA data using the above theoretical formalism. The transversity distribution functions and the Collins FFs are parametrized at an initial energy scale. A χ^2 minimization is then performed to simultaneously determine the parameters for the transversity distributions and Collins FFs. For the uncertainty estimation, we use the replica method.

According to Eq. (15) and the evolution equation (48), the Collins asymmetry in SIDIS process can be written as

$$A_{UT}^{\sin(\phi_h+\phi_s)} = M_h \frac{\sum_q e_q^2 \int_0^\infty \frac{bdb}{2\pi} bJ_1\left(\frac{b|P_{h\perp}|}{z}\right) R^2(b,Q) h_{1,q\leftarrow h_1}(x,b) H_{1,q\to h_2}^{\perp}(z,b)}{\sum_q e_q^2 \int_0^\infty \frac{bdb}{2\pi} J_0\left(\frac{b|P_{h\perp}|}{z}\right) R^2(b,Q) f_{1,q\leftarrow h_1}(x,b) D_{1,q\to h_2}(z,b)}, \tag{59}$$

where μ_i and ζ_i dependencies are suppressed for concise expressions. The same convention is used in the following discussions. The world SIDIS Collins asymmetry data $A_{UT}^{\sin(\phi_h+\phi_s)}$ in the analysis are summarized in Table III.

Similarly, according to Eqs. (21), (22), (23), and (48), the Collins asymmetry in the SIA process is written as

$$A_0^{UL} = \frac{\langle \sin^2\theta\rangle}{\langle 1+\cos^2\theta\rangle}(P_U - P_L), \tag{60}$$

where

$$P_\alpha(z_1,z_2,P_{h\perp}) = \frac{\sum_{h_1,h_2}^{\alpha}\sum_q e_q^2 \int_0^\infty dbb^3 M_{h_1} M_{h_2} J_2(P_{h\perp}b/z_1) R^2(b,Q) H_{q\to h_1}^{\perp}(z_1,b) H_{\bar q\to h_2}^{\perp}(z_2,b)}{\sum_{h_1,h_2}^{\alpha}\sum_q e_q^2 \int_0^\infty dbbJ_0(P_{h\perp}b/z_1) R^2(b,Q) D_{1,q\to h_1}(z_1,b) D_{1,\bar q\to h_2}(z_2,b)}, \tag{61}$$

where $\alpha = U(L)$ represents the final-state hadron h_1 and h_2 in unlike sign (like sign). The world SIA Collins asymmetry data A_0^{UL} in the analysis are summarized in Table IV.

The transversity distribution functions and the Collins FFs in Eqs. (59) and (61) can be expressed into a similar form to the unpolarized ones in Eq. (54) as

TABLE III. The world SIDIS data used in our analysis.

Dataset	Target	Beam	Data points	Reaction	Measurement
COMPASS [23]	^{6}LiD	160 GeV μ^+	92	$\mu^+d \to \mu^+\pi^+X$ $\mu^+d \to \mu^+\pi^-X$ $\mu^+d \to \mu^+K^+X$ $\mu^+d \to \mu^+K^-X$	$A_{UT}^{\sin(\phi_h+\phi_s-\pi)}$
COMPASS [24]	NH_3	160 GeV μ^+	92	$\mu^+p \to \mu^+\pi^+X$ $\mu^+p \to \mu^+\pi^-X$ $\mu^+p \to \mu^+K^+X$ $\mu^+p \to \mu^+K^-X$	$A_{UT}^{\sin(\phi_h+\phi_s-\pi)}$
HERMES [22]	H_2	27.6 GeV $e^\pm$	80	$e^\pm p \to e^\pm\pi^+X$ $e^\pm p \to e^\pm\pi^-X$ $e^\pm p \to e^\pm K^+X$ $e^\pm p \to e^\pm K^-X$	$A_{UT}^{\sin(\phi_h+\phi_s)}$
JLab [25]	^{3}He	5.9 GeV e^-	8	$e^-n \to e^-\pi^+X$ $e^-n \to e^-\pi^-X$	$\epsilon A_{UT}^{\sin(\phi_h+\phi_s)}$
JLab [26]	^{3}He	5.9 GeV e^-	5	$e^{-3}\mathrm{He} \to e^-K^+X$ $e^{-3}\mathrm{He} \to e^-K^-X$	$\epsilon A_{UT}^{\sin(\phi_h+\phi_s)}$

$$h_{1,q\leftarrow h}(x,b) = \sum_{q'}\int_x^1 \frac{dy}{y} C_{q\leftarrow q'}(y,b,\mu_0) \times h_{1,q'\leftarrow h}\left(\frac{x}{y},\mu_0\right) h_{\mathrm{NP}}(x,b), \quad (62)$$

$$H^\perp_{1,q\to h}(z,b) = \frac{1}{z^2}\sum_{q'}\int_z^1 \frac{dy}{y} y^2 \mathbb{C}_{q\to q'}(y,b,\mu_0) \times \hat{H}^{(3)}_{1,q'\to h}\left(\frac{z}{y},\mu_0\right) H_{\mathrm{NP}}(z,b), \quad (63)$$

where $h_{\mathrm{NP}}(x,b)$ and $H_{\mathrm{NP}}(z,b)$ are nonperturbative functions, $h_{1,q'\leftarrow h}(x,\mu_0)$ and $\hat{H}^{(3)}_{1,q'\to h}(z,\mu_0)$ are collinear transversity distribution functions and twist-3 FFs, and μ_0 is chosen as 2 GeV. The coefficients $C(\mathbb{C})$ are considered at the leading order [50]:

$$C(\mathbb{C})_{q\leftarrow q'} = \delta_{qq'}\delta(1-y). \quad (64)$$

Then we have

$$h_{1,q\leftarrow p}(x,b) = h_{1,q\leftarrow p}(x,\mu_0) h_{\mathrm{NP}}(x,b), \quad (65)$$

$$H^\perp_{1,q\to h}(z,b) = \frac{1}{z^2}\hat{H}^{(3)}_{1,q\to h}(z,\mu_0) H_{\mathrm{NP}}(z,b), \quad (66)$$

where $h_{1,q\leftarrow p}(x,b)$ are the transversity distributions of the proton, while the transversity distributions of the neutron, the deuteron, and the ^{3}He are approximated by $h_{1,q\leftarrow p}(x,b)$ assuming the isospin symmetry and neglecting the nuclear modification, with explicit relations provided in Appendix E.

Then we parametrize $h_{1,q\leftarrow p}(x,\mu_0)$ and $\hat{H}^{(3)}_{1,q\to h}(z,\mu_0)$ as

$$h_{1,u\leftarrow p}(x,\mu_0) = N_u \frac{(1-x)^{\alpha_u}x^{\beta_u}(1+\epsilon_u x)}{n(\beta_u,\epsilon_u,\alpha_u)} \times f_{1,u\leftarrow p}(x,\mu_0), \quad (67)$$

$$h_{1,d\leftarrow p}(x,\mu_0) = N_d \frac{(1-x)^{\alpha_d}x^{\beta_d}(1+\epsilon_d x)}{n(\beta_d,\epsilon_d,\alpha_d)} \times f_{1,d\leftarrow p}(x,\mu_0), \quad (68)$$

$$h_{1,\bar{u}\leftarrow p}(x,\mu_0) = N_{\bar{u}} \frac{(1-x)^{\alpha_{\bar{u}}}x^{\beta_{\bar{u}}}(1+\epsilon_{\bar{u}} x)}{n(\beta_{\bar{u}},\epsilon_{\bar{u}},\alpha_{\bar{u}})} \times (f_{1,u\leftarrow p}(x,\mu_0) - f_{1,\bar{u}\leftarrow p}(x,\mu_0)), \quad (69)$$

TABLE IV. The world SIA data used in our analysis.

Dataset	Energy	Dependence	Data points	Reaction
BELLE [27]	10.58 GeV	z	16	$e^+e^- \to \pi\pi X$
BABAR [28]	10.6 GeV	z	36	$e^+e^- \to \pi\pi X$
		$P_{h\perp}$	9	$e^+e^- \to \pi\pi X$
BABAR [29]	10.6 GeV	z	48	$e^+e^- \to \pi\pi X$
		z		$e^+e^- \to \pi KX$
		z		$e^+e^- \to KKX$
BESIII [30]	3.68 GeV	z	6	$e^+e^- \to \pi\pi X$
		$P_{h\perp}$	5	$e^+e^- \to \pi\pi X$

TABLE V. Free parameters for the transversity parametrizations.

Transversity	r	β	ϵ	α	N
u	r_u	β_u	ϵ_u	α_u	N_u
d	r_d	β_d	ϵ_d	α_d	N_d
$\bar{u}$	r_{sea}	0	0	0	$N_{\bar{u}}$
$\bar{d}$	r_{sea}	0	0	0	$N_{\bar{d}}$

TABLE VI. Free parameters for the parametrizations of Collins FFs. The label "f" and "u" stand for favored and unfavored, respectively.

Collins	η_1	η_3	η_4	β	ϵ	α	N
π_{fav}	η^{π}_{1f}	η^{π}_{3f}	η^{π}_{4f}	β^{π}_{f}	0	α^{π}_{f}	N^{π}_{f}
π_{unf}	η^{π}_{1u}	η^{π}_{3u}	η^{π}_{4u}	β^{π}_{u}	0	α^{π}_{u}	N^{π}_{u}
K_{fav}	η^{K}_{1f}	0	η^{K}_{4f}	β^{K}_{f}	0	α^{K}_{f}	N^{K}_{f}
K_{unf}	η^{K}_{1u}	0	η^{K}_{4u}	β^{K}_{u}	0	α^{K}_{u}	N^{K}_{u}

TABLE VII. The values of free parameters out of the fit to the world SIDIS and SIA data. The central values are the averaged result from 1000 replicas, and the uncertainties are the standard deviation from 1000 replicas. The values of r and η are provided in unit of GeV^2 and the others are unitless.

Transversity	Value	Collins	Value	Collins	Value
r_u	$0.12^{+0.04}_{-0.04}$	η^{π}_{1f}	$0.06^{+0.02}_{-0.01}$	β^{K}_{u}	$9.18^{+15.5}_{-7.59}$
r_d	$0.14^{+0.85}_{-0.11}$	η^{π}_{3f}	$0.09^{+0.12}_{-0.03}$	α^{π}_{f}	$1.83^{+0.45}_{-0.31}$
$r_{\rm sea}$	$0.70^{+1.43}_{-0.38}$	η^{π}_{4f}	$3.27^{+2.60}_{-0.77}$	α^{π}_{u}	$6.11^{+0.85}_{-1.22}$
β_u	$1.13^{+0.38}_{-0.32}$	η^{π}_{1u}	$0.03^{+0.01}_{-0.01}$	α^{K}_{f}	$0.70^{+1.68}_{-0.51}$
β_d	$3.43^{+8.58}_{-1.74}$	η^{π}_{3u}	$0.04^{+0.02}_{-0.02}$	α^{K}_{u}	$28.21^{+44.14}_{-22.15}$
ϵ_u	$0.17^{+4.44}_{-1.42}$	η^{π}_{4u}	$0.005^{+0.013}_{-0.002}$	N^{π}_{f}	$0.007^{+0.003}_{-0.002}$
ϵ_d	$1.17^{+4.47}_{-2.72}$	η^{K}_{1f}	$0.03^{+0.03}_{-0.02}$	N^{π}_{u}	$-3.83^{+1.06}_{-4.00}$
α_u	$0.28^{+1.04}_{-0.40}$	η^{K}_{4f}	$1.15^{+5.71}_{-0.94}$	N^{K}_{f}	$0.06^{+0.10}_{-0.04}$
α_d	$5.77^{+28.18}_{-4.91}$	η^{K}_{1u}	$0.02^{+0.08}_{-0.02}$	N^{K}_{u}	$-0.02^{+0.01}_{-0.05}$
N_u	$0.34^{+0.69}_{-0.36}$	η^{K}_{4u}	$0.71^{+3.80}_{-0.61}$		
N_d	$-1.37^{+1.23}_{-3.60}$	β^{π}_{f}	$2.82^{+1.17}_{-0.64}$		
$N_{\bar{u}}$	$-0.12^{+0.06}_{-0.46}$	β^{π}_{u}	$-0.23^{+0.24}_{-0.34}$		
$N_{\bar{d}}$	$0.10^{+0.47}_{-0.16}$	β^{K}_{f}	$-0.38^{+1.31}_{-0.37}$		

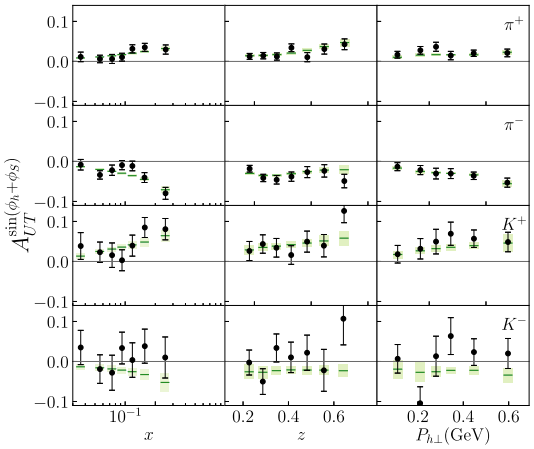

FIG. 3. Comparison of HERMES Collins asymmetry data [22] to theoretical calculations for π^+, π^-, K^+, and K^- productions from a proton target. The green lines are the central value calculated from the fit, and the bands represent the one standard deviation of the calculated asymmetries by using 1000 replicas.

$$h_{1,\bar{d}\leftarrow p}(x,\mu_0) = N_{\bar{d}}\frac{(1-x)^{\alpha_{\bar{d}}}x^{\beta_{\bar{d}}}(1+\epsilon_{\bar{d}}x)}{n(\beta_{\bar{d}},\epsilon_{\bar{d}},\alpha_{\bar{d}})} \times (f_{1,d\leftarrow p}(x,\mu_0) - f_{1,\bar{d}\leftarrow p}(x,\mu_0)), \quad (70)$$

$$\hat{H}^{(3)}_{1,q\to h}(z,\mu_0) = N^h_q\frac{(1-z)^{\alpha^h_q}z^{\beta^h_q}(1+\epsilon^h_q z)}{n(\beta^h_q,\epsilon^h_q,\alpha^h_q)}, \quad (71)$$

where $f_{1,q\leftarrow p}(x,\mu_0)$ are collinear unpolarized PDFs. We did not impose the Soffer bound [51] while parametrizing the transversity functions, leaving space to test it by experimental data. The nonperturbative functions $h_{\rm NP}$ and $H_{\rm NP}$ for each flavor take the same form as $f_{\rm NP}$ and $D_{\rm NP}$ in Eqs. (57) and (58). However, since the existing world data with limited amount are not precise enough to determine so many parameters, we simplify the parametrization form by setting $\eta_2 = \eta_1$ for the each Collins FF,

TABLE VIII. The χ^2 values for different datasets. N is the number of data points for each experimental dataset.

SIDIS	Dependence	N	χ^2/N	SIA	Channel	Dependence	N	χ^2/N
COMPASS [23]	x	36	1.2	BELLE [27]	$\pi\pi$	z	16	0.9
COMPASS [23]	z	32	0.7	*BABAR* [28]	$\pi\pi$	z	36	0.7
COMPASS [23]	$P_{h\perp}$	24	1.3	*BABAR* [28]	$\pi\pi$	$P_{h\perp}$	9	1.8
COMPASS [24]	x	36	1.3	*BABAR* [29]	$\pi\pi$	z	16	0.7
COMPASS [24]	z	32	0.9	*BABAR* [29]	πK	z	16	0.7
COMPASS [24]	$P_{h\perp}$	24	0.7	*BABAR* [29]	KK	z	16	0.6
HERMES [22]	x	28	0.8	BESIII [30]	$\pi\pi$	z	6	3.3
HERMES [22]	z	28	1.0	BESIII [30]	$\pi\pi$	$P_{h\perp}$	5	0.9
HERMES [22]	$P_{h\perp}$	24	0.9					
JLab [25,26]	x	13	1.1					
Total		277	0.99				120	0.95

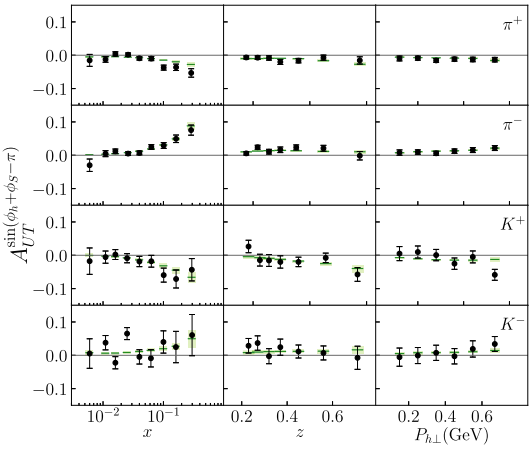

FIG. 4. Comparison of COMPASS Collins asymmetry data [24] to theoretical calculations for π^+, π^-, K^+, and K^- productions from a proton target. The markers and bands have the same meaning as in Fig. 3.

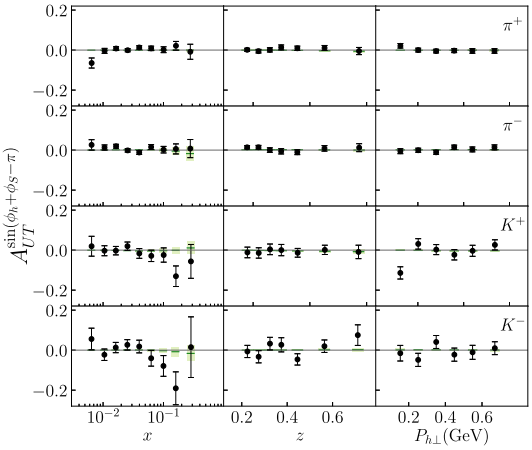

FIG. 5. Comparison of COMPASS Collins asymmetry data [23] to theoretical calculations for π^+, π^-, K^+ and K^- productions from a deuteron target. The markers and bands have the same meaning as in Fig. 3.

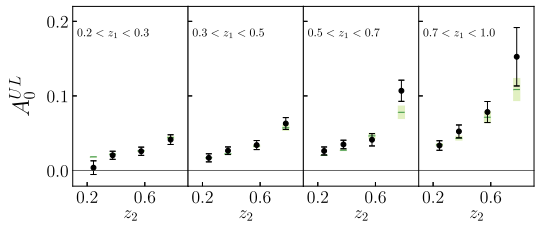

FIG. 7. Comparison of BELLE $\pi\pi$ channel Collins asymmetry data [27] to theoretical calculations in the SIA process. The markers and bands have the same meaning as in Fig. 3.

$\lambda_1 = \lambda_2 = r$ and $\lambda_3 = \lambda_4 = \lambda_5 = 0$ for the transversity distribution of each flavor. Furthermore, we use the same $r_{\bar{u}} = r_{\bar{d}} = r_{\rm sea}$ for $\bar{u}$ and $\bar{d}$ transversity distributions and set the s and $\bar{s}$ transversity distributions to zero. The factor

$$n(\beta,\epsilon,\alpha) = \frac{\Gamma(\alpha+1)(2+\alpha+\beta+\epsilon+\epsilon\beta)\Gamma(\beta+1)}{\Gamma(\beta+\alpha+3)} \tag{72}$$

is introduced to reduce the correlation between the parameters controlling the shape and the normalization.

Because of the limited number of independent observables, the Collins functions are assumed to be favored and unfavored cases for pion and kaon, as follows:

$$\begin{aligned}
&H^{\perp}_{1,u\to\pi^+} = H^{\perp}_{1,\bar{d}\to\pi^+} = H^{\perp}_{1,d\to\pi^-} = H^{\perp}_{1,\bar{u}\to\pi^-} \equiv H^{\pi}_{fav},\\
&H^{\perp}_{1,d\to\pi^+} = H^{\perp}_{1,\bar{u}\to\pi^+} = H^{\perp}_{1,u\to\pi^-} = H^{\perp}_{1,\bar{d}\to\pi^-} = H^{\perp}_{1,s\to\pi^+}\\
&\qquad = H^{\perp}_{1,\bar{s}\to\pi^+} = H^{\perp}_{1,s\to\pi^-} = H^{\perp}_{1,\bar{s}\to\pi^-} \equiv H^{\pi}_{unf},\\
&H^{\perp}_{1,u\to K^+} = H^{\perp}_{1,\bar{u}\to K^-} = H^{\perp}_{1,\bar{s}\to K^+} = H^{\perp}_{1,s\to K^-} \equiv H^{K}_{fav},\\
&H^{\perp}_{1,d\to K^+} = H^{\perp}_{1,\bar{d}\to K^+} = H^{\perp}_{1,d\to K^-} = H^{\perp}_{1,\bar{d}\to K^-} = H^{\perp}_{1,\bar{u}\to K^+}\\
&\qquad = H^{\perp}_{1,u\to K^-} = H^{\perp}_{1,s\to K^+} = H^{\perp}_{1,\bar{s}\to K^-} \equiv H^{K}_{unf}.
\end{aligned} \tag{73}$$

As listed in Tables V and VI, there are in total 35 free parameters in this fit.

Because of limited statistics and phase space coverage, many experimental data were analyzed in one-dimensional binning in variables of x, z, and/or $P_{h\perp}$, respectively.

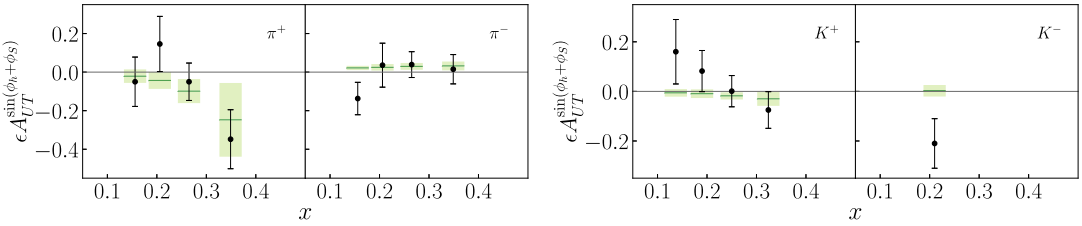

FIG. 6. Comparison of JLab Collins asymmetry data [25,26] to theoretical calculations for π^+, π^-, K^+ and K^- productions from a ^{3}He target. The asymmetries for π^+ and π^- productions in the left panel have been extracted at the neutron level, while the kaon results are at ^{3}He level due to limited statistics. The markers and bands have the same meaning as in Fig. 3.

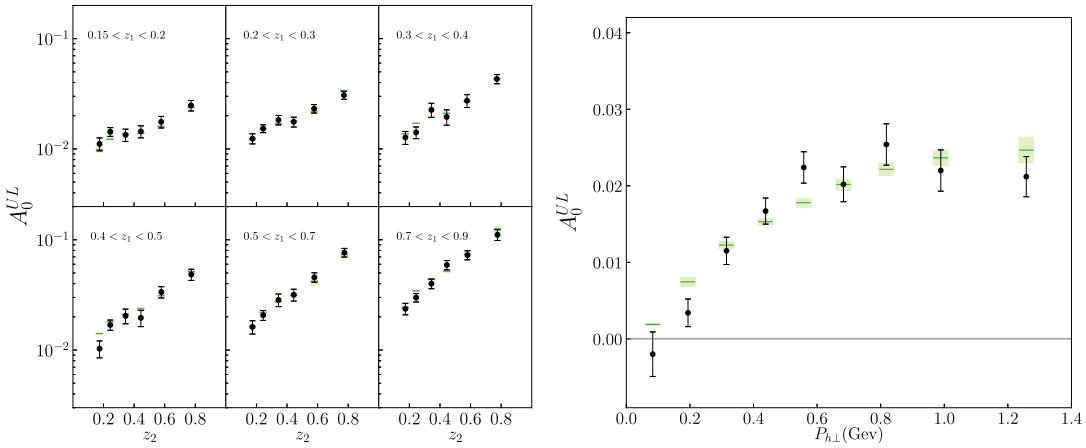

FIG. 8. Comparison of *BABAR* $\pi\pi$ channel Collins asymmetry data [28] to theoretical calculations in the SIA process as a function of z (left) and $P_{h\perp}$ (right). The markers and bands have the same meaning as in Fig. 3.

In order to maximally use the data information from binning in different kinematic variables and meanwhile to avoid a duplicate usage of the same dataset, we assign a weight factor when calculating the χ^2 from each dataset. The COMPASS and HERMES datasets are given the weight of $1/3$, since the binnings in x, z, and $P_{h\perp}$ are provided, respectively, from the same collected events. The *BABAR* [28] and BESIII data are given the weight of $1/2$, since the binnings in z and $P_{h\perp}$ are provided, respectively, from the same events.

To estimate the uncertainty, we randomly shift the central values of the data points by Gaussian distributions with the Gaussian widths given by the experimental uncertainties and then perform a fit to the smeared data. By repeating this procedure, we create 1000 replicas. The central values of the parameters together with their uncertainties out of the fit are listed in Table VII. The total χ^2/N of the fit and its value for various experimental datasets are listed in Table VIII. Here, N denotes the number of experimental data points. The comparisons between experimental data and the theoretical calculations using the 1000 replicas are shown in Figs. 3–10.

The first transverse moment of Collins FF $H_1^{\perp(1)}(z)$ and that of the transversity distribution $h_1(x)$ are defined, respectively, as

$$H_1^{\perp(1)}(z) = \int d^2\boldsymbol{p}_T \frac{p_T^2}{2z^2 M_h^2} H_1^{\perp}(z, p_T), \tag{74}$$

$$h_1(x) = \int d^2\boldsymbol{k}_\perp h_1(x, k_\perp). \tag{75}$$

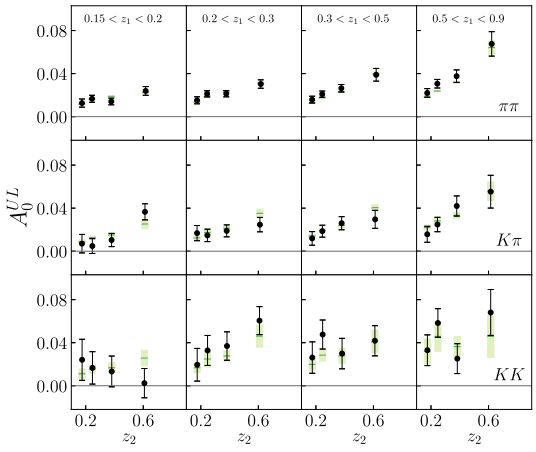

FIG. 9. Comparison of *BABAR* $\pi\pi$, $K\pi$, and KK channels Collins asymmetry data [29] to theoretical calculations in the SIA process. The markers and bands have the same meaning as in Fig. 3.

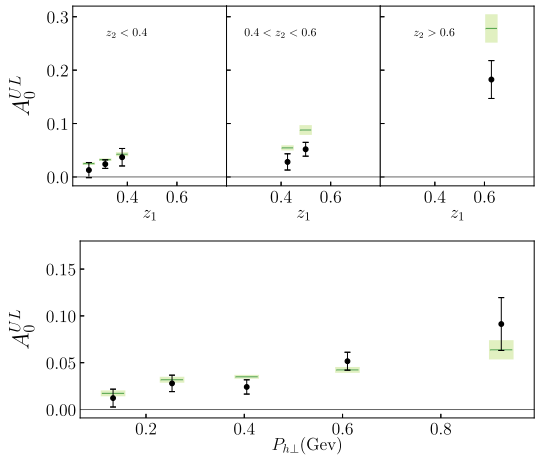

FIG. 10. Comparison of BESIII $\pi\pi$ channel Collins asymmetry data [30] to theoretical calculations in the SIA process as a function of z (left) and $P_{h\perp}$ (right). The markers and bands have the same meaning as in Fig. 3.

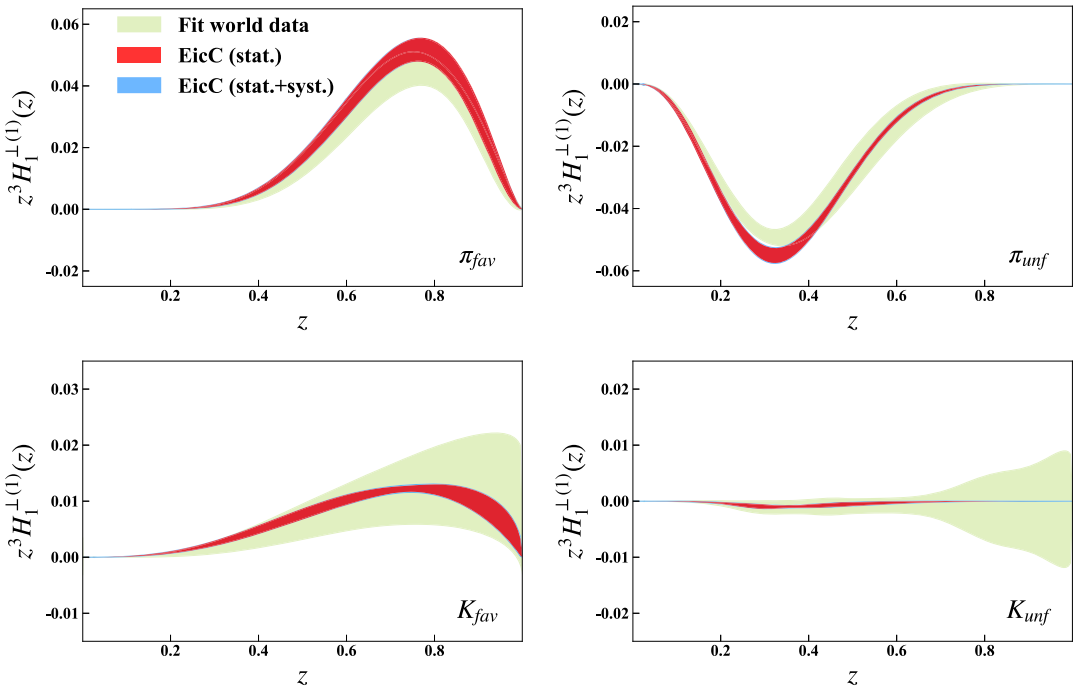

FIG. 11. Collins functions as defined in Eq. (74) with the $\boldsymbol{p}_T$ integral truncated at 1 GeV and $Q = 2$ GeV. The green bands represent the uncertainties of the fit to the world SIDIS and SIA data, the red bands represent the EicC projections with only statistical uncertainties, and the blue bands represent the EicC projections including systematic uncertainties as described in the text.

Their results are shown in Figs. 11 and 12. Considering the uncertainty band, the fitting results out of the world data do cross the Soffer bound at large x. However, one cannot make a conclusion with current uncertainties. It needs to be tested with precise data in the future. One can observe that the $\bar{u}$ transversity distribution favors a negative value about 2σ away from zero, while the $\bar{d}$ transversity distribution is consistent with zero in the 1σ band. The u and d transversity distributions are consistent with previous global analyses within the uncertainties.

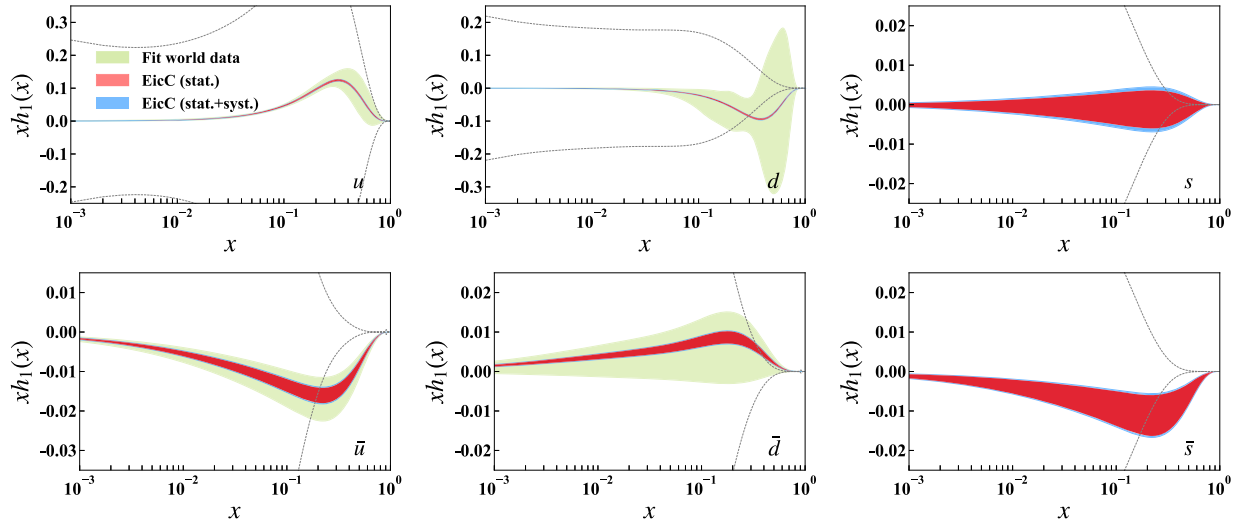

FIG. 12. Transversity functions as defined in Eq. (75) with the $\boldsymbol{k}_\perp$ integral truncated at 1 GeV and $Q = 2$ GeV. The green bands represent the uncertainties of the fit to the world SIDIS and SIA data, the red bands represent the EicC projections with only statistical uncertainties, and the blue bands represent the EicC projections including systematic uncertainties as described in the text. The Soffer bound [51] which is calculated by using CT18NLO [53] unpolarized PDFs and D. de Florian, R. Sassot, M. Stratmann, and W. Vogelsang (DSSV) [54] helicity PDFs is shown as black dashed curves.

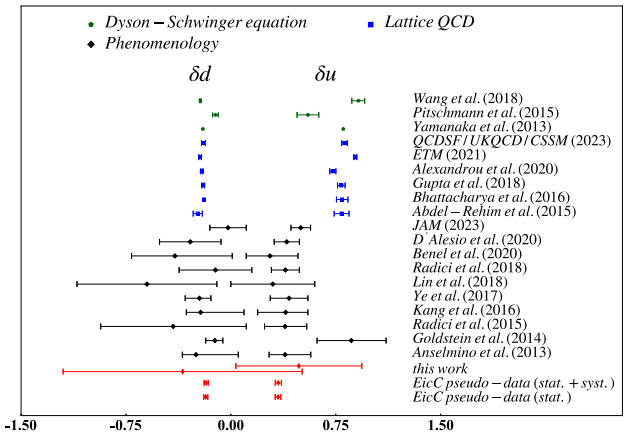

FIG. 13. Tensor charge for u quark and d quark from our study at 68% C.L. along with the results from Dyson-Schwinger equation calculations [55–57], lattice QCD calculations [6–11], and phenomenological extractions from data [33–35,37–41,58,59].

The tensor charge can be evaluated from the integral of the transversity distributions as

$$\delta u = \int_0^1 dx (h_1^u(x) - h_1^{\bar{u}}(x)), \tag{76}$$

$$\delta d = \int_0^1 dx (h_1^d(x) - h_1^{\bar{d}}(x)), \tag{77}$$

and the isovector combination is given by

$$g_T = \delta u - \delta d. \tag{78}$$

The extracted tensor charges from our analysis are compared with the results from previous phenomenological

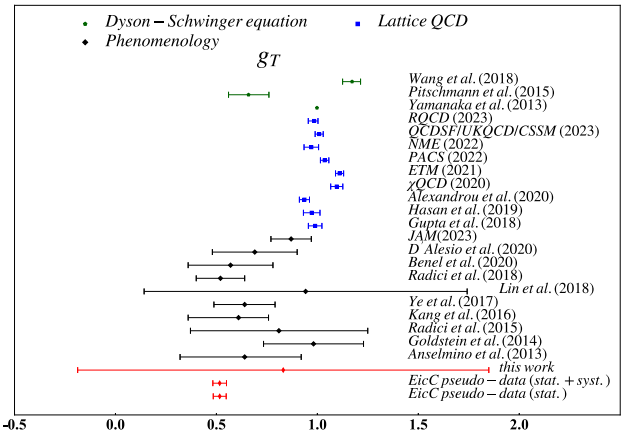

FIG. 14. Tensor charge g_T from our study at 68% C.L. along with the results from Dyson-Schwinger equation calculations [55–57], lattice QCD calculations [5–9,60–63], and phenomenological extractions from data [33–35,37–41,58,59].

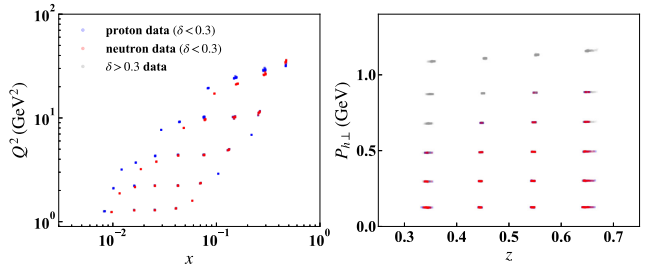

FIG. 15. Kinematic distributions of the EicC pseudodata in $x - Q^2$ (left) and $z - P_{h\perp}$ (right) planes. Each bin is plotted as a point at the bin center kinematic values. The blue points are the proton data with $\delta < 0.3$, the red points are the neutron data with $\delta < 0.3$, and the gray points are the data with $\delta > 0.3$.

studies, lattice calculations, and Dyson-Schwinger equations are shown in Figs. 13 and 14. It is not a surprise that the uncertainties of our result are larger than those from previous phenomenological studies of SIDIS and SIA data, because we include more flavors, $\bar{u}$ and $\bar{d}$, and, thus, the functions are less constrained. We note that the negative $\bar{u}$ transversity distribution shift δu as well as g_T to a greater value, though with large uncertainties. The tension between lattice QCD calculations and TMD phenomenological extractions disappears when the antiquark transversity distributions are taken into account. In previous works, such tension was found to be resolved by imposing the lattice data in the fit [35,40,42].

IV. EicC PROJECTIONS ON TRANSVERSITY DISTRIBUTIONS AND COLLINS FFs

The EicC SIDIS pseudodata are produced by the Monte Carlo event generator SIDIS-RC EvGen [52], in which the unpolarized SIDIS differential cross section used in the generator is derived from a global fit to the multiplicity data from HERMES and COMPASS experiments. Based on the EicC conceptual design, the electron beam energy is 3.5 GeV, the proton beam energy is 20 GeV, and the ^{3}He beam energy is 40 GeV. Physical cuts $Q^2 > 1$ GeV^2, $0.3 < z < 0.7$, $W > 5$ GeV, and $W' > 2$ GeV are adopted to select events in the deep inelastic region. We estimate the statistics by assuming 50 fb^{-1} for ep collisions and 50 fb^{-1} for e^3He collisions. Based on the designed instantaneous

TABLE IX. Free parameters for the transversity parametrization for the fit to EicC pseudodata.

Transversity	r	β	ϵ	α	N
u	r_u	β_u	ϵ_u	α_u	N_u
d	r_d	β_d	ϵ_d	α_d	N_d
$\bar{u}$	$r_{\rm sea}$	0	0	0	$N_{\bar{u}}$
$\bar{d}$	$r_{\rm sea}$	0	0	0	$N_{\bar{d}}$
s	$r_{\rm sea}$	0	0	0	N_s
$\bar{s}$	$r_{\rm sea}$	0	0	0	$N_{\bar{s}}$

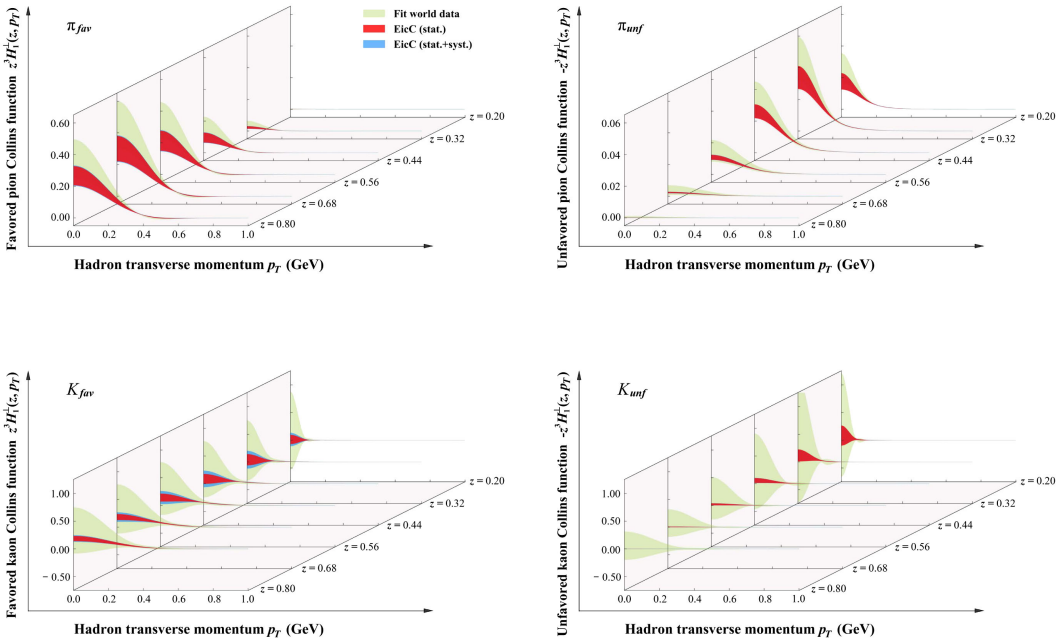

FIG. 16. The transverse momentum distribution of the Collins functions at different z values and $Q = 2$ GeV. The green bands represent the uncertainties of the fit to the world SIDIS and SIA data, the red bands represent the EicC projections with only statistical uncertainties, and the blue bands represent the EicC projections including systematic uncertainties as described in the text.

luminosity of 2×10^{33} cm^{-2} s^{-1}, it is estimated that 50 fb^{-1} of accumulated luminosity can be attained in approximately one year of operation. Keeping the statistical uncertainty at 10^{-3} level, we obtain 4627 data points in four-dimensional bins in x, Q^2, z, and $P_{h\perp}$. The EicC pseudodata provide significantly more data points with higher precision, enabling us to impose more rigorous kinematic cuts for a more precise selection of data in the TMD region. In this study, only small transverse momentum data with $\delta = |P_{h\perp}|/(zQ) < 0.3$ are selected. After applying this data selection cut, there are 1347 EicC pseudodata points left. The distributions of all 4627 EicC pseudodata points are shown in Fig. 15, where the colored points are selected in the fit while the gray ones are not. The Collins asymmetry values of the EicC pseudodata are calculated using the central value of the 1000 replicas from the fit to the world data. For systematic uncertainties, we assign 3% relative uncertainty for the proton data mainly due to the precision from beam polarimetry and 5% relative uncertainty for the neutron data mainly due to the precision from beam polarimetry and nuclear effects. Total uncertainties are evaluated via the quadrature combination of statistical uncertainties and systematic uncertainties.

The precise EicC data with wide kinematics coverage allow us to adopt a more flexible parametrization of the transversity functions. Therefore, we open the channels of s and $\bar{s}$ transversity functions in the fit with the following parametrizations:

$$h_{1,s\leftarrow p}(x,b) = N_s \frac{(1-x)^{\alpha_s} x^{\beta_s}(1+\epsilon_s x)}{n(\beta_s,\epsilon_s,\alpha_s)} \exp(-r_{\rm sea} b^2) \times (f_{1,u\leftarrow p}(x,\mu_0) - f_{1,\bar{u}\leftarrow p}(x,\mu_0)), \quad (79)$$

$$h_{1,\bar{s}\leftarrow p}(x,b) = N_{\bar{s}} \frac{(1-x)^{\alpha_{\bar{s}}} x^{\beta_{\bar{s}}}(1+\epsilon_{\bar{s}} x)}{n(\beta_{\bar{s}},\epsilon_{\bar{s}},\alpha_{\bar{s}})} \exp(-r_{\rm sea} b^2) \times (f_{1,u\leftarrow p}(x,\mu_0) - f_{1,\bar{u}\leftarrow p}(x,\mu_0)). \quad (80)$$

Then, we have 37 free parameters for the EicC pseudodata fit, as listed in Tables IX and VI. To estimate the impact of the EicC on the extraction of the transversity distribution functions and Collins FFs, we perform a simultaneous fit to the world data and the EicC pseudodata as described above. Following the same procedure, 300 replicas are created by randomly shifting the values according to the simulated statistical uncertainty and total uncertainty, respectively. The EicC projections for $H_1^{\perp(1)}(z)$, $h_1(x)$, and tensor charges are shown in Figs. 11–14, respectively. The transverse momentum distribution of the Collins and transversity functions are shown in Figs. 16 and 17 via slices at various x and z values. While considering the dominant systematic sources, the statistical uncertainty still dominates the results, so the blue band (obtained including systematic uncertainty) and red band (obtained with only statistical uncertainty) almost coincide. The mean value of transversity functions for u and d quark with different Q is shown in Fig. 18, where one can observe that the

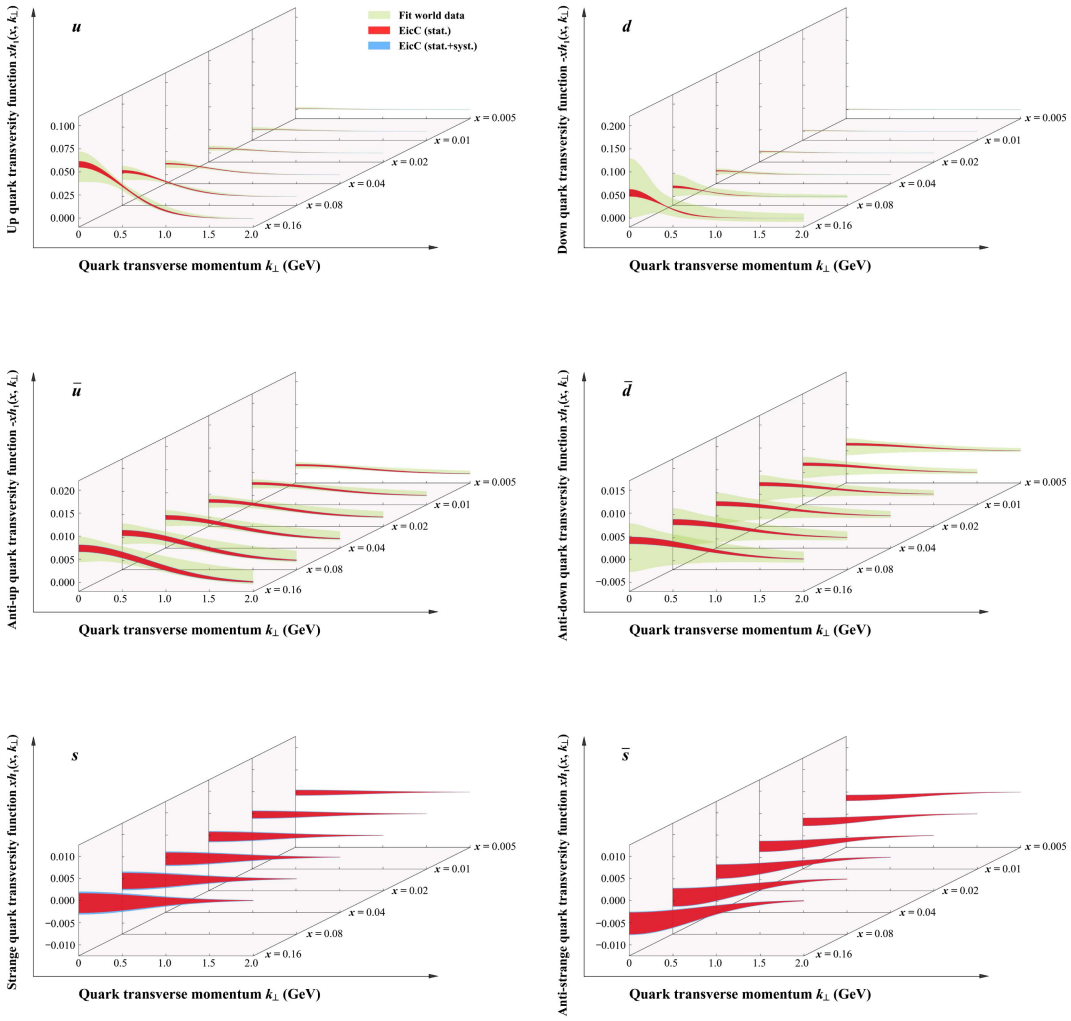

FIG. 17. The transverse momentum distribution of the transversity functions at different x values and $Q = 2$ GeV. The green bands represent the uncertainties of the fit to the world SIDIS and SIA data, the red bands represent the EicC projections with only statistical uncertainties, and the blue bands represent the EicC projections including systematic uncertainties as described in the text.

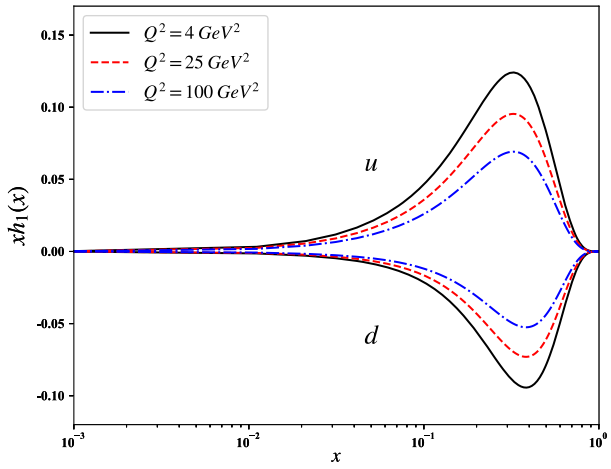

FIG. 18. The mean value of transversity functions for u and d quark as defined in Eq. (75) with different Q^2.

transversity functions are expected to have stronger signals in the kinematics region covered by the EicC.

V. SUMMARY

In this paper, we present a global analysis of transversity distribution functions and Collins FFs by simultaneously fitting to SIDIS and SIA data within the TMD factorization. Nonzero $\bar{u}$ and $\bar{d}$ transversity distributions are taken into account. The result favors a negative $\bar{u}$ transversity distribution with a significance of 2 standard deviations, while no hint is found for nonvanishing $\bar{d}$ transversity distribution with the current accuracy. The results of u and d transversity distributions and the results of Collins FFs are consistent with previous phenomenological analyses by other groups. The tensor charges evaluated from the moment of transversity distributions out of the global data fit are consistent with lattice QCD calculations as well as other global fits within the uncertainties, and, thus, no

tension exists between lattice calculation and TMD extractions once antiquark contributions are taken into account. We note that these findings are based on the exploratory measurements worldwide. To make decisive conclusions, data with high precision in a wide phase space coverage are desired, which can be achieved at the future JLab programs and the EICs.

Based on the fit of existing world data, we investigated the impact of the proposed EicC on the extraction of transversity TMDs and the Collins FFs. With the EicC pseudodata, one can extract the transversity functions at high precision for various quark flavors and, thus, determine the proton tensor charge with precision comparable to the lattice calculations.

Moreover, the precise and wide kinematics coverage of the EicC pseudodata allows us to use much more flexible parametrizations, which can minimize the bias on the transversity function, and have a cleaner selection of data for TMDs study by applying a more strict requirement on $\delta \equiv |P_{h\perp}|/(zQ)$ to restrict data in the low transverse momentum region, suitable for the application of TMD factorization. The proposed EicC SIDIS program will fill the kinematics gap between the coverage by the JLab 12-GeV program and by the EIC at BNL. Combining all these measurements, we will be able to have a complete physical picture of the three-dimensional structures of the nucleon. On the other hand, in the $x - Q^2$ region covered by the EicC, the transverse single spin asymmetries caused by transversity distributions are expected to have significant signals based on our current knowledge. This would be an advantage for the study of nucleon structures at a collider with a moderate center-of-mass energy [64].

ACKNOWLEDGMENTS

C. Z. is grateful for the valuable discussions with Zhi Hu at the Institute of Modern Physics. This work is supported by the Strategic Priority Research Program of the Chinese Academy of Sciences under Grant No. XDB34000000, the Guangdong Major Project of Basic and Applied Basic Research No. 2020B0301030008, the Guangdong Provincial Key Laboratory of Nuclear Science with No. 2019B121203010, the National Natural Science Foundation of China under Contracts No. 12175117, No. 12321005, No. 11975127, and No. 12061131006, and by the Shandong Provincial Natural Science Foundation under Contract No. ZFJH202303. The authors also acknowledge the computing resources available at the Southern Nuclear Science Computing Center.

APPENDIX A: EVOLUTION AND RESUMMATION

Through the integrability condition (also known as the Collins-Soper equation [65])

$$\zeta \frac{d}{d\zeta}\gamma_F(\mu,\zeta) = -\mu\frac{d}{d\mu}\mathcal{D}(\mu,b) = -\Gamma_{\rm cusp}(\mu), \tag{A1}$$

the anomalous dimension $\gamma_F(\mu,\zeta)$ can be written as

$$\gamma_F(\mu,\zeta) = \Gamma_{\rm cusp}(\mu)\ln\left(\frac{\mu^2}{\zeta}\right) - \gamma_V(\mu), \tag{A2}$$

where $\Gamma_{\rm cusp}(\mu)$ is the cusp anomalous dimension and $\gamma_V(\mu)$ is the finite part of the renormalization of the vector form factor. These factors can be expanded using a series expansion in terms of the strong coupling constant α_s:

$$\Gamma_{\rm cusp}(\mu) = \sum_{n=0}^{\infty} a_s^{n+1}\Gamma_n, \tag{A3}$$

$$\gamma_V(\mu) = \sum_{n=1}^{\infty} a_s^n \gamma_n, \tag{A4}$$

where $a_s = \alpha_s/(4\pi)$. When $\mu \gg \Lambda_{\rm QCD}$, the coefficients Γ_n and γ_n can be calculated via perturbative QCD order by order, and up to two-loop order, they are

$$\Gamma_0 = 4C_F, \tag{A5}$$

$$\Gamma_1 = 4C_F\left[\left(\frac{67}{9} - \frac{\pi^2}{3}\right)C_A - \frac{20}{9}T_R N_f\right], \tag{A6}$$

$$\gamma_1 = -6C_F, \tag{A7}$$

$$\begin{aligned}\gamma_2 = {} & C_F^2(-3 + 4\pi^2 - 48\zeta_3) \\ & + C_F C_A\left(-\frac{961}{27} - \frac{11\pi^2}{3} + 52\zeta_3\right) \\ & + C_F T_R N_f\left(\frac{260}{27} + \frac{4\pi^2}{3}\right),\end{aligned} \tag{A8}$$

where $C_F = 4/3$, $C_A = 3$, and $T_R = 1/2$ are color factors of the SU(3) and $\zeta_3 \approx 1.202$ is the Apéry constant. The number of active quark flavors is set as $N_f = 4$ in this work ignoring heavy quark contributions.

Meanwhile, the integrability condition Eq. (A1) is satisfied with the renormalization group equation

$$\mu^2\frac{d\mathcal{D}(\mu,b)}{d\mu^2} = \frac{\Gamma_{\rm cusp}(\mu)}{2}, \tag{A9}$$

and consequently the rapidity anomalous dimension $\mathcal{D}(\mu,b)$ can be calculated at small b perturbatively with a similar expression in power of a_s:

$$\mathcal{D}_{\rm pert}(\mu,b) = \sum_{n=0}^{\infty} a_s^n d_n(\mathbf{L}_\mu), \tag{A10}$$

where

$$\mathbf{L}_\mu = \ln\left(\frac{\mu^2 b^2}{4e^{-2\gamma_E}}\right), \tag{A11}$$

with the Euler-Mascheroni constant γ_E. The function $d_n(\mathbf{L}_\mu)$ can be expressed up to two-loop order as

$$d_0(\mathbf{L}_\mu) = 0, \tag{A12}$$

$$d_1(\mathbf{L}_\mu) = \frac{\Gamma_0}{2}\mathbf{L}_\mu, \tag{A13}$$

$$d_2(\mathbf{L}_\mu) = \frac{\Gamma_0}{4}\beta_0\mathbf{L}_\mu^2 + \frac{\Gamma_1}{2}\mathbf{L}_\mu + d_2(0), \tag{A14}$$

where

$$d_2(0) = C_F C_A\left(\frac{404}{27} - 14\zeta_3\right)\frac{112}{27}T_R N_f C_F. \tag{A15}$$

To improve the convergence properties of $\mathcal{D}_{\rm pert}(\mu, b)$, we employ the resummed expression. The resummed expression $\mathcal{D}_{\rm resum}$ can be obtained by adopting the approach outlined in [66]:

$$\begin{aligned}\mathcal{D}_{\rm resum}(\mu, b) = &-\frac{\Gamma_0}{2\beta_0}\ln(1-X) + \frac{a_s}{2\beta_0(1-X)}\left[-\frac{\beta_1\Gamma_0}{\beta_0}(\ln(1-X)+X) + \Gamma_1 X\right] \\ &+ \frac{a_s^2}{(1-X)^2}\left[\frac{\Gamma_0\beta_1^2}{4\beta_0^3}(\ln^2(1-X) - X^2) + \frac{\beta_1\Gamma_1}{4\beta_0^2}(X^2 - 2X - 2\ln(1-X))\right. \\ &\left. + \frac{\Gamma_0\beta_2}{4\beta_0^2}X^2 - \frac{\Gamma_2}{4\beta_0}X(X-2) + C_F C_A\left(\frac{404}{27} - 14\zeta_3\right) - \frac{112}{27}T_R N_f C_F\right],\end{aligned} \tag{A16}$$

where $X = \beta_0 a_s \mathbf{L}_\mu$ and the QCD β function can be expressed as

$$\beta(\alpha_s) = -2\alpha_s\sum_{n=1}^{\infty}\beta_{n-1}\left(\frac{\alpha_s}{4\pi}\right)^n, \tag{A17}$$

$$\begin{aligned}\beta_0 &= \frac{11}{3}C_A - \frac{4}{3}T_R N_f, \\ \beta_1 &= \frac{34}{3}C_A^2 - \frac{20}{3}C_A T_R N_f - 4C_F T_R N_f, \\ \beta_2 &= \frac{2857}{54}C_A^3 + \left(2C_F^2 - \frac{205}{9}C_F C_A - \frac{1415}{27}C_A^2\right)T_R N_f \\ &\quad + \left(\frac{44}{9}C_F + \frac{158}{27}C_A\right)T_R^2 N_f^2.\end{aligned} \tag{A18}$$

$\mathcal{D}_{\rm resum}$ is valid only in the small-b region. Therefore, a nonperturbative function is required to model the large-b contribution, which is adopted as $d_{\rm NP}$ with the form of a linear function according to Refs. [67–71]:

$$d_{\rm NP}(b) = c_0 b b^*, \tag{A19}$$

where

$$b^* = \frac{b}{\sqrt{1 + b^2/B_{\rm NP}^2}}. \tag{A20}$$

For arbitrary large b, one has $b^* < B_{\rm NP}$ and $b^* \approx b$ for small b. Finally, $\mathcal{D}(\mu, b)$ can be expanded as

$$\mathcal{D}(\mu, b) = \mathcal{D}_{\rm resum}(\mu, b^*) + d_{\rm NP}(b). \tag{A21}$$

According to the ζ prescription [48], the TMD evolution can be written as the following simple form:

$$R[b; (\mu_i, \zeta_i) \to (Q, Q^2)] = \left(\frac{Q^2}{\zeta_\mu(Q, b)}\right)^{-\mathcal{D}(Q,b)}, \tag{A22}$$

where $\zeta_\mu(Q, b)$ is obtained by solving the equation

$$\frac{d\ln\zeta_\mu(\mu, b)}{d\ln\mu^2} = \frac{\gamma_F(\mu, \zeta_\mu(\mu, b))}{2\mathcal{D}(\mu, b)}, \tag{A23}$$

with using Eq. (A21) as an input and the boundary conditions

$$\mathcal{D}(\mu_0, b) = 0, \qquad \gamma_F(\mu_0, \zeta_\mu(\mu_0, b)) = 0. \tag{A24}$$

In order to utilize the perturbative solution in the small-b region for $\zeta_\mu(\mu, b)$, we apply the formulas as in Ref. [72]:

$$\begin{aligned}\zeta_\mu(\mu, b) = &\zeta_\mu^{\rm pert}(\mu, b)e^{-b^2/B_{\rm NP}^2} \\ &+ \zeta_\mu^{\rm exact}(\mu, b)(1 - e^{-b^2/B_{\rm NP}^2}).\end{aligned} \tag{A25}$$

The perturbative solution of Eq. (A23) can be written as

$$\zeta_\mu^{\rm pert}(\mu, b) = \frac{2\mu e^{-\gamma_E}}{b}e^{-v(\mu,b)}, \tag{A26}$$

which is consistent with the pQCD result by construction [73]. Up to two-loop order, $v(\mu, b)$ can be written as

$$v(\mu,b)=\frac{\gamma_1}{\Gamma_0}+a_s\left[\frac{\beta_0}{12}\boldsymbol{L}_\mu^2+\frac{\gamma_2+d_2(0)}{\Gamma_0}-\frac{\gamma_1\Gamma_1}{\Gamma_0^2}\right]. \tag{A27}$$

And, according to the approach in Ref. [72], $\zeta_\mu^{\rm exact}(\mu,b)$ can be written as

$$\zeta_\mu^{\rm exact}(\mu,b)=\mu^2 e^{-g(\mu,b)/\mathcal{D}(\mu,b)}. \tag{A28}$$

Up to two-loop order, $g(\mu,b)$ can be written as

$$\begin{aligned}g(\mu,b)=&\frac{1}{a_s}\frac{\Gamma_0}{2\beta_0^2}\left\{e^{-p}-1+p+a_s\left[\frac{\beta_1}{\beta_0}\left(e^{-p}-1+p-\frac{p^2}{2}\right)-\frac{\Gamma_1}{\Gamma_0}(e^{-p}-1+p)+\frac{\beta_0\gamma_1}{\Gamma_0}p\right]\right.\\&\left.+a_s^2\left[\left(\frac{\Gamma_1^2}{\Gamma_0^2}-\frac{\Gamma_2}{\Gamma_0}\right)(\cosh p-1)+\left(\frac{\beta_1\Gamma_1}{\beta_0\Gamma_0}-\frac{\beta_2}{\beta_0}\right)(\sinh p-p)+\left(\frac{\beta_0\gamma_2}{\Gamma_0}-\frac{\beta_0\gamma_1\Gamma_1}{\Gamma_0^2}\right)(e^p-1)\right]\right\},\end{aligned} \tag{A29}$$

where

$$p=\frac{2\beta_0\mathcal{D}(\mu,b)}{\Gamma_0}. \tag{A30}$$

APPENDIX B: FOURIER TRANSFORMS FOR PDFs AND FFs

The Fourier transforms for PDFs and FFs are

$$\begin{aligned}f_1(x,k_\perp)&=\frac{1}{4\pi^2}\int e^{i\boldsymbol{b}\cdot\boldsymbol{k}_\perp}f_1(x,b)d^2\boldsymbol{b}\\&=\frac{1}{2\pi}\int_0^{+\infty}J_0(bk_\perp)f_1(x,b)bdb,\end{aligned} \tag{B1}$$

$$\begin{aligned}f_1(x,b)&=\int e^{-i\boldsymbol{b}\cdot\boldsymbol{k}_\perp}f_1(x,k_\perp)d^2\boldsymbol{k}_\perp\\&=2\pi\int_0^{+\infty}J_0(bk_\perp)f_1(x,k_\perp)k_\perp dk_\perp,\end{aligned} \tag{B2}$$

$$\begin{aligned}h_1(x,k_\perp)&=\frac{1}{4\pi^2}\int e^{i\boldsymbol{b}\cdot\boldsymbol{k}_\perp}h_1(x,b)d^2\boldsymbol{b}\\&=\frac{1}{2\pi}\int_0^{+\infty}J_0(bk_\perp)h_1(x,b)bdb,\end{aligned} \tag{B3}$$

$$\begin{aligned}h_1(x,b)&=\int e^{-i\boldsymbol{b}\cdot\boldsymbol{k}_\perp}h_1(x,k_\perp)d^2\boldsymbol{k}_\perp\\&=2\pi\int_0^{+\infty}J_0(bk_\perp)h_1(x,k_\perp)k_\perp dk_\perp,\end{aligned} \tag{B4}$$

$$\begin{aligned}D_1(z,zp_\perp)&=\frac{1}{4\pi^2}\int e^{-i\boldsymbol{b}\cdot\boldsymbol{p}_\perp}D_1(z,b)d^2\boldsymbol{b}\\&=\frac{1}{2\pi}\int_0^{+\infty}J_0(bp_\perp)D_1(z,b)bdb,\end{aligned} \tag{B5}$$

$$\begin{aligned}D_1(z,b)&=\int e^{i\boldsymbol{b}\cdot\boldsymbol{p}_\perp}D_1(z,zp_\perp)d^2\boldsymbol{p}_\perp\\&=2\pi\int_0^{+\infty}J_0(bp_\perp)D_1(x,zp_\perp)p_\perp dp_\perp,\end{aligned} \tag{B6}$$

$$\begin{aligned}\frac{\boldsymbol{p}_\perp}{M_h}H_1^\perp(z,zp_\perp)&=\frac{1}{4\pi^2}\int e^{-i\boldsymbol{b}\cdot\boldsymbol{p}_\perp}i\boldsymbol{b}M_hH_1^\perp(z,b)d^2\boldsymbol{b},\\H_1^\perp(z,zp_\perp)&=\frac{M_h^2}{2\pi p_\perp}\int_0^\infty J_1(bp_\perp)b^2H_1^\perp(z,b)db,\end{aligned} \tag{B7}$$

$$\begin{aligned}iM_h\boldsymbol{b}H_1^\perp(z,b)&=\int e^{i\boldsymbol{b}\cdot\boldsymbol{p}_\perp}\frac{\boldsymbol{p}_\perp}{M_h}H_1^\perp(z,zp_\perp)d^2\boldsymbol{p}_\perp,\\H_1^\perp(z,b)&=\frac{2\pi}{M_h^2b}\int_0^\infty J_1(bp_\perp)p_\perp^2H_1^\perp(z,zp_\perp)dp_\perp,\end{aligned} \tag{B8}$$

where hadron h and flavor q dependencies in TMDs are omitted for convenience in Appendix B and $\boldsymbol{p}_\perp$ is the transverse momentum of the final-state quark.

APPENDIX C: EXPRESSION OF STRUCTURE FUNCTIONS

For the SIDIS process, we have

$$\begin{aligned} F_{UU,T} &= \mathcal{C}[f_1 D_1] \\ &= x\sum_q e_q^2 \int d^2\boldsymbol{p}_T d^2\boldsymbol{k}_\perp \delta^{(2)}(\boldsymbol{p}_T + z\boldsymbol{k}_\perp - \boldsymbol{P}_{h\perp}) f_{1,q\leftarrow h_1}(x,k_\perp) D_{1,q\to h_2}(z,p_T) \\ &= x\sum_q \frac{e_q^2}{4\pi^2} \int d^2\boldsymbol{p}_\perp d^2\boldsymbol{k}_\perp d^2\boldsymbol{b} e^{i\boldsymbol{b}\cdot(\boldsymbol{p}_\perp - \boldsymbol{k}_\perp + \boldsymbol{P}_{h\perp}/z)} f_{1,q\leftarrow h_1}(x,k_\perp) D_{1,q\to h_2}(z,zp_\perp) \\ &= x\sum_q \frac{e_q^2}{2\pi} \int_0^\infty b J_0(bP_{h\perp}/z) f_{1,q\leftarrow h_1}(x,b) D_{1,q\to h_2}(z,b) db, \end{aligned} \tag{C1}$$

$$\begin{aligned} F_{UT}^{\sin(\phi_h+\phi_S)} &= \mathcal{C}\left[\frac{\hat{\boldsymbol{h}}\cdot\boldsymbol{p}_T}{zM_h} h_1 H_1^\perp\right] \\ &= x\sum_q e_q^2 \int d^2\boldsymbol{p}_T d^2\boldsymbol{k}_\perp \delta^{(2)}(\boldsymbol{p}_T + z\boldsymbol{k}_\perp - \boldsymbol{P}_{h\perp}) \frac{\hat{\boldsymbol{h}}\cdot\boldsymbol{p}_T}{zM_h} h_{1,q\leftarrow h_1}(x,k_\perp) H^\perp_{1,q\to h_2}(z,p_T) \\ &= -x\sum_q \frac{e_q^2}{4\pi^2} \int d^2\boldsymbol{b} d^2\boldsymbol{p}_\perp d^2\boldsymbol{k}_\perp e^{i\boldsymbol{b}\cdot\boldsymbol{p}_\perp} e^{-i\boldsymbol{b}\cdot\boldsymbol{k}_\perp} e^{i\boldsymbol{b}\cdot\boldsymbol{P}_{h\perp}/z} \frac{\hat{\boldsymbol{h}}\cdot\boldsymbol{p}_\perp}{M_h} h_{1,q\leftarrow h_1}(x,k_\perp) H^\perp_{1,q\to h_2}(z,zp_\perp) \\ &= x\sum_q e_q^2 \int_0^\infty \frac{M_h}{2\pi} J_1(bP_{h\perp}/z) b^2 h_{1,q\leftarrow h_1}(x,b) H^\perp_{1,q\to h_2}(z,b) db, \end{aligned} \tag{C2}$$

where one uses the following equation:

$$-\boldsymbol{p}_\perp = \boldsymbol{p}_T/z, \qquad \boldsymbol{P}_{h\perp} = \boldsymbol{p}_T + z\boldsymbol{k}_\perp. \tag{C3}$$

For the SIA process, we have

$$\begin{aligned} F_{uu}^{h_1h_2} &= \mathcal{C}[D_1 D_1] \\ &= \sum_q e_q^2 \int \frac{d^2\boldsymbol{p}_{1T}}{z_1^2}\frac{d^2\boldsymbol{p}_{2T}}{z_2^2} \delta^{(2)}\left(-\frac{\boldsymbol{p}_{1T}}{z_1} - \frac{\boldsymbol{p}_{2T}}{z_2} + \frac{\boldsymbol{P}_{h\perp}}{z_1}\right) D_{1,q\to h_1}(z_1,p_{1T}) D_{1,\bar{q}\to h_2}(z_2,p_{2T}) \\ &= \frac{1}{4\pi^2}\sum_q e_q^2 \int d^2\boldsymbol{p}_{1\perp} d^2\boldsymbol{p}_{2\perp} e^{i\boldsymbol{b}\cdot(\boldsymbol{p}_{1\perp} + \boldsymbol{p}_{2\perp} + \boldsymbol{P}_{h\perp}/z_1)} D_{1,q\to h_1}(z_1, z_1 p_{1\perp}) D_{1,\bar{q}\to h_2}(z_2, z_2 p_{2\perp}) d^2\boldsymbol{b} \\ &= \frac{1}{2\pi}\sum_q e_q^2 \int J_0(P_{h\perp}b/z_1) D_{1,q\to h_1}(z_1,b) D_{1,\bar{q}\to h_2}(z_2,b) b db, \end{aligned} \tag{C4}$$

$$\begin{aligned} F_{\text{Collins}}^{h_1h_2} &= \mathcal{C}\left[\frac{2(\hat{\boldsymbol{h}}\cdot\boldsymbol{p}_{1T})(\hat{\boldsymbol{h}}\cdot\boldsymbol{p}_{2T}) - \boldsymbol{p}_{1T}\cdot\boldsymbol{p}_{2T}}{z_1 z_2 M_{h_1} M_{h_2}} H_1^\perp H_1^\perp\right] \\ &= 2F_{col1}^{h_1h_2} - F_{col2}^{h_1h_2} \\ &= \frac{M_{h_1}M_{h_2}}{2\pi}\sum_q e_q^2 \int J_2(P_{h\perp}b/z_1) H^\perp_{1,q\to h_1}(z_1,b) H^\perp_{1,\bar{q}\to h_2}(z_2,b) b^3 db, \end{aligned} \tag{C5}$$

where

$$F^{h_1h_2}_{col1} = \sum_q e_q^2 \int \frac{d^2\boldsymbol{p}_{1T}}{z_1^2}\frac{d^2\boldsymbol{p}_{2T}}{z_2^2}\delta^{(2)}\left(-\frac{\boldsymbol{p}_{1T}}{z_1}-\frac{\boldsymbol{p}_{2T}}{z_2}+\frac{\boldsymbol{P}_{h\perp}}{z_1}\right)\frac{\hat{\boldsymbol{h}}\cdot\boldsymbol{p}_{1T}}{z_1 M_{h_1}}H^{\perp}_{1,q\to h_1}(z_1,p_{1T})\frac{\hat{\boldsymbol{h}}\cdot\boldsymbol{p}_{2T}}{z_2 M_{h_2}}H^{\perp}_{1,\bar{q}\to h_2}(z_2,p_{2T})$$
$$= \sum_q e_q^2 \int d^2\boldsymbol{p}_{1\perp}d^2\boldsymbol{p}_{2\perp}\delta^{(2)}\left(\boldsymbol{p}_{1\perp}+\boldsymbol{p}_{2\perp}+\frac{\boldsymbol{P}_{h\perp}}{z_1}\right)\frac{\hat{\boldsymbol{h}}\cdot\boldsymbol{p}_{1\perp}}{M_{h_1}}H^{\perp}_{1,q\to h_1}(z_1,z_1p_{1\perp})\frac{\hat{\boldsymbol{h}}\cdot\boldsymbol{p}_{2\perp}}{M_{h_2}}H^{\perp}_{1,\bar{q}\to h_2}(z_2,z_2p_{2\perp})$$
$$= \frac{M_{h_1}M_{h_2}}{2\pi}\sum_q e_q^2\int_0^\infty db\, b^3(J_2(bP_{h\perp}/z_1)-J_1(bP_{h\perp}/z_1)/(bP_{h\perp}/z_1))H^{\perp}_{1,q\to h_1}(z_1,b)H^{\perp}_{1,\bar{q}\to h_2}(z_2,b), \tag{C6}$$

$$F^{h_1h_2}_{col2} = \sum_q e_q^2 \int \frac{d^2\boldsymbol{p}_{1T}}{z_1^2}\frac{d^2\boldsymbol{p}_{2T}}{z_2^2}\delta^{(2)}\left(-\frac{\boldsymbol{p}_{1T}}{z_1}-\frac{\boldsymbol{p}_{2T}}{z_2}+\frac{\boldsymbol{P}_{h\perp}}{z_1}\right)\frac{\boldsymbol{p}_{1T}\cdot\boldsymbol{p}_{2T}}{z_1z_2M_{h_1}M_{h_2}}H^{\perp}_{1,q\to h_1}(z_1,p_{1T})H^{\perp}_{1,\bar{q}\to h_2}(z_2,p_{2T})$$
$$= \sum_q e_q^2 \int d^2\boldsymbol{p}_{1\perp}d^2\boldsymbol{p}_{2\perp}\delta^{(2)}\left(\boldsymbol{p}_{1\perp}+\boldsymbol{p}_{2\perp}+\frac{\boldsymbol{P}_{h\perp}}{z_1}\right)\frac{\boldsymbol{p}_{1\perp}\cdot\boldsymbol{p}_{2\perp}}{M_{h_1}M_{h_2}}H^{\perp}_{1,q\to h_1}(z_1,z_1p_{1\perp})H^{\perp}_{1,\bar{q}\to h_2}(z_2,z_2p_{2\perp})$$
$$= -\frac{M_{h_1}M_{h_2}}{2\pi}\sum_a e_q^2\int dbb^3J_0(bP_{h_\perp}/z_1)H^{\perp}_{1,q\to h_1}(z_1,b)H^{\perp}_{1,\bar{q}\to h_2}(z_2,b), \tag{C7}$$

where $J_n(X)$ is Bessel functions and we use the following relation:

$$2\frac{J_1(X)}{X} = J_2(X)+J_0(X), \tag{C8}$$

and similar to Eq. (C3) one can have the following equation:

$$-\boldsymbol{p}_{1\perp} = \boldsymbol{p}_{1T}/z_1, \qquad -\boldsymbol{p}_{2\perp} = \boldsymbol{p}_{2T}/z_2,$$
$$\boldsymbol{P}_{h\perp}/z_1 = \boldsymbol{p}_{1T}/z_1+\boldsymbol{p}_{2T}/z_2. \tag{C9}$$

APPENDIX D: EXPRESSION OF MATCHING FUNCTIONS

For TMD PDFs, the coefficient function C up to NLO is [48]

$$C_{f\leftarrow f'}(x,b,\mu) = \delta(1-x)\delta_{ff'} + a_s(\mu)(-\boldsymbol{L}_\mu P^{(1)}_{f\leftarrow f'}+C^{(1,0)}_{f\leftarrow f'}), \tag{D1}$$

where

$$C^{(1,0)}_{q\leftarrow q'}(x) = C_F\left[2(1-x)-\delta(1-x)\frac{\pi^2}{6}\right]\delta_{qq'}, \tag{D2}$$

$$C^{(1,0)}_{q\leftarrow g}(x) = 2x(1-x), \tag{D3}$$

$$P^{(1)}_{q\leftarrow q'}(x) = 2C_F\left[\frac{2}{(1-x)_+}-1-x+\frac{3}{2}\delta(1-x)\right]\delta_{qq'}, \tag{D4}$$

$$P^{(1)}_{q\leftarrow g}(x) = 1-2x+2x^2. \tag{D5}$$

For TMD FFs, the matching coefficient $\mathbb{C}$ up to NLO follows the same pattern as in Eq. (D1) with the replacement of the PDF Dokshitzer-Gribov-Lipatov-Altarelli-Parisi (DGLAP) kernels $P^{(1)}_{f\leftarrow f'}(x)$ by the FF DGLAP kernels [74]:

$$\mathbb{P}^{(1)}_{q\to q'}(z) = \frac{2C_F}{z^2}\left(\frac{1+z^2}{1-z}\right)_+\delta_{qq'}, \tag{D6}$$

$$\mathbb{P}^{(1)}_{q\to g}(z) = \frac{2C_F}{z^2}\frac{1+(1-z)^2}{z}, \tag{D7}$$

and the replacement of $C^{(1,0)}_{f\leftarrow f'}(x)$ by [48]

$$\mathbb{C}^{(1,0)}_{q\to q'}(z) = \frac{C_F}{z^2}\left[2(1-z)+\frac{4(1+z^2)\ln z}{1-z}-\delta(1-z)\frac{\pi^2}{6}\right]\delta_{qq'}, \tag{D8}$$

$$\mathbb{C}^{(1,0)}_{q\to g}(z) = \frac{2C_F}{z^2}\left[z+2(1+(1-z)^2)\frac{\ln z}{z}\right]. \tag{D9}$$

The "+" prescription is defined as

$$\int_{x_0}^1 dx[g(x)]_+f(x) = \int_0^1 dxg(x)[f(x)\Theta(x-x_0)-f(1)], \tag{D10}$$

where $\Theta(x-x_0)$ is the Heaviside step function.

APPENDIX E: TRANSVERSITY FUNCTION WITH DIFFERENT TARGET

The isospin symmetry is also assumed to relate the transversity function of the neutron and the transversity function of the proton as (μ_i and ζ_i dependencies in TMDs are omitted for convenience)

$$\begin{aligned} h_{1,u\leftarrow n}(x,b) &= h_{1,d\leftarrow p}(x,b), \\ h_{1,\bar{u}\leftarrow n}(x,b) &= h_{1,\bar{d}\leftarrow p}(x,b), \\ h_{1,d\leftarrow n}(x,b) &= h_{1,u\leftarrow p}(x,b), \\ h_{1,\bar{d}\leftarrow n}(x,b) &= h_{1,\bar{u}\leftarrow p}(x,b), \\ h_{1,s\leftarrow n}(x,b) &= h_{1,s\leftarrow p}(x,b), \\ h_{1,\bar{s}\leftarrow n}(x,b) &= h_{1,\bar{s}\leftarrow p}(x,b). \end{aligned} \tag{E1}$$

Since a free neutron target is not available for SIDIS experiments, the polarized deuteron and polarized ^{3}He are commonly used to obtain parton distributions in the neutron. As an approximation, the transversity functions of the deuteron and the ^{3}He are set via the weighted combination of the proton transversity function and the neutron transversity function. For a deuteron, the transversity function is expressed as

$$h_{1,q\leftarrow d}(x,b) = \frac{P_d^n h_{1,q\leftarrow n}(x,b) + P_d^p h_{1,q\leftarrow p}(x,b)}{2}, \tag{E2}$$

where $P_d^n = P_d^p = 0.925$ are effective polarizations of the neutron and the proton in a polarized deuteron [75]. Similarly, the transversity function of a ^{3}He is

$$h_{1,\mathrm{q}\leftarrow{}^3\mathrm{He}}(x,b) = \frac{P_{\mathrm{He}}^n h_{1,q\leftarrow n}(x,b) + 2P_{\mathrm{He}}^p h_{1,q\leftarrow p}(x,b)}{3}, \tag{E3}$$

where $P_{\mathrm{He}}^n = 0.86$ and $P_{\mathrm{He}}^p = -0.028$ are effective polarizations of the neutron and the proton in a polarized ^{3}He [76].

This parametrization setup is applied for both the fit to world SIDIS data and the fit to EicC pseudodata.

[1] J. C. Collins, D. E. Soper, and G. F. Sterman, Transverse momentum distribution in Drell-Yan pair and W and Z boson production, Nucl. Phys. **B250**, 199 (1985).

[2] J. C. Collins, D. E. Soper, and G. F. Sterman, Factorization of hard processes in QCD, Adv. Ser. Dir. High Energy Phys. **5**, 1 (1989).

[3] J. Ashman *et al.* (European Muon Collaboration), A measurement of the spin asymmetry and determination of the structure function g_1 in deep inelastic muon-proton scattering, Phys. Lett. B **206**, 364 (1988).

[4] J. Ashman *et al.* (European Muon Collaboration), An investigation of the spin structure of the proton in deep inelastic scattering of polarized muons on polarized protons, Nucl. Phys. **B328**, 1 (1989).

[5] D. Horkel, Y. Bi, M. Constantinou, T. Draper, J. Liang, K.-F. Liu, Z. Liu, and Y.-B. Yang (χQCD Collaboration), Nucleon isovector tensor charge from lattice QCD using chiral fermions, Phys. Rev. D **101**, 094501 (2020).

[6] R. E. Smail *et al.*, Constraining beyond the Standard Model nucleon isovector charges, Phys. Rev. D **108**, 094511 (2023).

[7] C. Alexandrou, M. Constantinou, K. Hadjiyiannakou, K. Jansen, and F. Manigrasso, Flavor decomposition of the nucleon unpolarized, helicity, and transversity parton distribution functions from lattice QCD simulations, Phys. Rev. D **104**, 054503 (2021).

[8] C. Alexandrou, S. Bacchio, M. Constantinou, J. Finkenrath, K. Hadjiyiannakou, K. Jansen, G. Koutsou, and A. Vaquero Aviles-Casco, Nucleon axial, tensor, and scalar charges and σ-terms in lattice QCD, Phys. Rev. D **102**, 054517 (2020).

[9] R. Gupta, Y.-C. Jang, B. Yoon, H.-W. Lin, V. Cirigliano, and T. Bhattacharya, Isovector charges of the nucleon from $2+1+1$-flavor lattice QCD, Phys. Rev. D **98**, 034503 (2018).

[10] T. Bhattacharya, V. Cirigliano, S. Cohen, R. Gupta, H.-W. Lin, and B. Yoon, Axial, scalar and tensor charges of the nucleon from $2+1+1$-flavor lattice QCD, Phys. Rev. D **94**, 054508 (2016).

[11] A. Abdel-Rehim *et al.*, Nucleon and pion structure with lattice QCD simulations at physical value of the pion mass, Phys. Rev. D **92**, 114513 (2015).

[12] A. Courtoy, S. Baeßler, M. González-Alonso, and S. Liuti, Beyond-standard-model tensor interaction and hadron phenomenology, Phys. Rev. Lett. **115**, 162001 (2015).

[13] T. Liu, Z. Zhao, and H. Gao, Experimental constraint on quark electric dipole moments, Phys. Rev. D **97**, 074018 (2018).

[14] X. Artru and M. Mekhfi, Transversely polarized parton densities, their evolution and their measurement, Z. Phys. C **45**, 669 (1990).

[15] R. L. Jaffe and X.-D. Ji, Chiral odd parton distributions and polarized Drell-Yan, Phys. Rev. Lett. **67**, 552 (1991).

[16] J. C. Collins, Fragmentation of transversely polarized quarks probed in transverse momentum distributions, Nucl. Phys. **B396**, 161 (1993).

[17] A. Bacchetta, F. A. Ceccopieri, A. Mukherjee, and M. Radici, Asymmetries involving dihadron fragmentation functions: From DIS to e^+e^- annihilation, Phys. Rev. D **79**, 034029 (2009).

[18] J. L. Cortes, B. Pire, and J. P. Ralston, Measuring the transverse polarization of quarks in the proton, Z. Phys. C **55**, 409 (1992).

[19] M. Anselmino, V. Barone, A. Drago, and N. N. Nikolaev, Accessing transversity via J/ψ production in polarized $p^{\uparrow}\bar{p}^{\uparrow}$ interactions, Phys. Lett. B **594**, 97 (2004).
[20] A. V. Efremov, K. Goeke, and P. Schweitzer, Transversity distribution function in hard scattering of polarized protons and antiprotons in the PAX experiment, Eur. Phys. J. C **35**, 207 (2004).
[21] B. Pasquini, M. Pincetti, and S. Boffi, Drell-Yan processes, transversity and light-cone wavefunctions, Phys. Rev. D **76**, 034020 (2007).
[22] A. Airapetian *et al.* (HERMES Collaboration), Azimuthal single- and double-spin asymmetries in semi-inclusive deep-inelastic lepton scattering by transversely polarized protons, J. High Energy Phys. 12 (2020) 010.
[23] M. Alekseev *et al.* (COMPASS Collaboration), Collins and Sivers asymmetries for pions and kaons in muon-deuteron DIS, Phys. Lett. B **673**, 127 (2009).
[24] C. Adolph *et al.* (COMPASS Collaboration), Collins and Sivers asymmetries in muonproduction of pions and kaons off transversely polarised protons, Phys. Lett. B **744**, 250 (2015).
[25] X. Qian *et al.* (Jefferson Lab Hall A Collaboration), Single spin asymmetries in charged pion production from semi-inclusive deep inelastic scattering on a transversely polarized ^{3}He target, Phys. Rev. Lett. **107**, 072003 (2011).
[26] Y. X. Zhao *et al.* (Jefferson Lab Hall A Collaboration), Single spin asymmetries in charged kaon production from semi-inclusive deep inelastic scattering on a transversely polarized ^{3}He target, Phys. Rev. C **90**, 055201 (2014).
[27] R. Seidl *et al.* (Belle Collaboration), Measurement of azimuthal asymmetries in inclusive production of hadron pairs in e^+e^- annihilation at $\sqrt{s} = 10.58$ GeV, Phys. Rev. D **78**, 032011 (2008); **86**, 039905(E) (2012).
[28] J. P. Lees *et al.* (*BABAR* Collaboration), Measurement of Collins asymmetries in inclusive production of charged pion pairs in e^+e^- annihilation at *BABAR*, Phys. Rev. D **90**, 052003 (2014).
[29] J. P. Lees *et al.* (*BABAR* Collaboration), Collins asymmetries in inclusive charged KK and $K\pi$ pairs produced in e^+e^- annihilation, Phys. Rev. D **92**, 111101 (2015).
[30] M. Ablikim *et al.* (BESIII Collaboration), Measurement of azimuthal asymmetries in inclusive charged dipion production in e^+e^- annihilations at $\sqrt{s} = 3.65$ GeV, Phys. Rev. Lett. **116**, 042001 (2016).
[31] A. Bacchetta, A. Courtoy, and M. Radici, First glances at the transversity parton distribution through dihadron fragmentation functions, Phys. Rev. Lett. **107**, 012001 (2011).
[32] A. Bacchetta, A. Courtoy, and M. Radici, First extraction of valence transversities in a collinear framework, J. High Energy Phys. 03 (2013) 119.
[33] M. Radici, A. Courtoy, A. Bacchetta, and M. Guagnelli, Improved extraction of valence transversity distributions from inclusive dihadron production, J. High Energy Phys. 05 (2015) 123.
[34] M. Radici and A. Bacchetta, First extraction of transversity from a global analysis of electron-proton and proton-proton data, Phys. Rev. Lett. **120**, 192001 (2018).
[35] C. Cocuzza, A. Metz, D. Pitonyak, A. Prokudin, N. Sato, and R. Seidl, First simultaneous global QCD analysis of dihadron fragmentation functions and transversity parton distribution functions, arXiv:2308.14857.
[36] M. Anselmino, M. Boglione, U. D'Alesio, A. Kotzinian, F. Murgia, A. Prokudin, and C. Turk, Transversity and Collins functions from SIDIS and e^+e^- data, Phys. Rev. D **75**, 054032 (2007).
[37] M. Anselmino, M. Boglione, U. D'Alesio, S. Melis, F. Murgia, and A. Prokudin, Simultaneous extraction of transversity and Collins functions from new SIDIS and e^+e^- data, Phys. Rev. D **87**, 094019 (2013).
[38] Z.-B. Kang, A. Prokudin, P. Sun, and F. Yuan, Extraction of quark transversity distribution and Collins fragmentation functions with QCD evolution, Phys. Rev. D **93**, 014009 (2016).
[39] Z. Ye, N. Sato, K. Allada, T. Liu, J.-P. Chen, H. Gao, Z.-B. Kang, A. Prokudin, P. Sun, and F. Yuan, Unveiling the nucleon tensor charge at Jefferson Lab: A study of the SoLID case, Phys. Lett. B **767**, 91 (2017).
[40] H.-W. Lin, W. Melnitchouk, A. Prokudin, N. Sato, and H. Shows, First Monte Carlo global analysis of nucleon transversity with lattice QCD constraints, Phys. Rev. Lett. **120**, 152502 (2018).
[41] U. D'Alesio, C. Flore, and A. Prokudin, Role of the Soffer bound in determination of transversity and the tensor charge, Phys. Lett. B **803**, 135347 (2020).
[42] J. Cammarota, L. Gamberg, Z.-B. Kang, J. A. Miller, D. Pitonyak, A. Prokudin, T. C. Rogers, and N. Sato (JAM Collaboration), Origin of single transverse-spin asymmetries in high-energy collisions, Phys. Rev. D **102**, 054002 (2020).
[43] L. Gamberg, M. Malda, J. A. Miller, D. Pitonyak, A. Prokudin, and N. Sato (JAM Collaboration), Updated QCD global analysis of single transverse-spin asymmetries: Extracting $\tilde{H}$, and the role of the Soffer bound and lattice QCD, Phys. Rev. D **106**, 034014 (2022).
[44] A. Accardi *et al.*, Electron ion collider: The next QCD frontier: Understanding the glue that binds us all, Eur. Phys. J. A **52**, 268 (2016).
[45] R. Abdul Khalek *et al.*, Science requirements and detector concepts for the electron-ion collider: EIC Yellow report, Nucl. Phys. **A1026**, 122447 (2022).
[46] D. P. Anderle *et al.*, Electron-ion collider in China, Front. Phys. (Beijing) **16**, 64701 (2021).
[47] A. Bacchetta, U. D'Alesio, M. Diehl, and C. A. Miller, Single-spin asymmetries: The Trento conventions, Phys. Rev. D **70**, 117504 (2004).
[48] I. Scimemi and A. Vladimirov, Non-perturbative structure of semi-inclusive deep-inelastic and Drell-Yan scattering at small transverse momentum, J. High Energy Phys. 06 (2020) 137.
[49] I. Scimemi, A. Tarasov, and A. Vladimirov, Collinear matching for Sivers function at next-to-leading order, J. High Energy Phys. 05 (2019) 125.
[50] M. G. Echevarria, I. Scimemi, and A. Vladimirov, Unpolarized transverse momentum dependent parton distribution and fragmentation functions at next-to-next-to-leading order, J. High Energy Phys. 09 (2016) 004.
[51] J. Soffer, Positivity constraints for spin-dependent parton distributions, Phys. Rev. Lett. **74**, 1292 (1995).
[52] https://github.com/TianboLiu/LiuSIDIS.
[53] T.-J. Hou *et al.*, Progress in the CTEQ-TEA NNLO global QCD analysis, arXiv:1908.11394.

[54] V. Bertone, S. Carrazza, and J. Rojo (APFEL), APFEL: A PDF evolution library with QED corrections, Comput. Phys. Commun. **185**, 1647 (2014).
[55] M. Pitschmann, C.-Y. Seng, C. D. Roberts, and S. M. Schmidt, Nucleon tensor charges and electric dipole moments, Phys. Rev. D **91**, 074004 (2015).
[56] N. Yamanaka, T. M. Doi, S. Imai, and H. Suganuma, Quark tensor charge and electric dipole moment within the Schwinger-Dyson formalism, Phys. Rev. D **88**, 074036 (2013).
[57] Q.-W. Wang, S.-X. Qin, C. D. Roberts, and S. M. Schmidt, Proton tensor charges from a Poincaré-covariant Faddeev equation, Phys. Rev. D **98**, 054019 (2018).
[58] G. R. Goldstein, J. O. Gonzalez Hernandez, and S. Liuti, Flavor dependence of chiral odd generalized parton distributions and the tensor charge from the analysis of combined π^0 and η exclusive electroproduction data, arXiv:1401.0438.
[59] J. Benel, A. Courtoy, and R. Ferro-Hernandez, A constrained fit of the valence transversity distributions from dihadron production, Eur. Phys. J. C **80**, 465 (2020).
[60] S. Park, R. Gupta, B. Yoon, S. Mondal, T. Bhattacharya, Y.-C. Jang, B. Joó, and F. Winter (NME Collaboration), Precision nucleon charges and form factors using $(2+1)$-flavor lattice QCD, Phys. Rev. D **105**, 054505 (2022).
[61] R. Tsuji, N. Tsukamoto, Y. Aoki, K.-I. Ishikawa, Y. Kuramashi, S. Sasaki, E. Shintani, and T. Yamazaki (PACS Collaboration), Nucleon isovector couplings in $N_f = 2+1$ lattice QCD at the physical point, Phys. Rev. D **106**, 094505 (2022).
[62] G. S. Bali, S. Collins, S. Heybrock, M. Löffler, R. Rödl, W. Söldner, and S. Weishäupl (RQCD Collaboration), Octet baryon isovector charges from $N_f = 2+1$ lattice QCD, Phys. Rev. D **108**, 034512 (2023).
[63] N. Hasan, J. Green, S. Meinel, M. Engelhardt, S. Krieg, J. Negele, A. Pochinsky, and S. Syritsyn, Nucleon axial, scalar, and tensor charges using lattice QCD at the physical pion mass, Phys. Rev. D **99**, 114505 (2019).
[64] S. M. Aybat, A. Prokudin, and T. C. Rogers, Calculation of TMD evolution for transverse single spin asymmetry measurements, Phys. Rev. Lett. **108**, 242003 (2012).
[65] J. C. Collins and D. E. Soper, Back-to-back jets: Fourier transform from B to K-transverse, Nucl. Phys. **B197**, 446 (1982).
[66] M. G. Echevarria, A. Idilbi, A. Schäfer, and I. Scimemi, Model-independent evolution of transverse momentum dependent distribution functions (TMDs) at NNLL, Eur. Phys. J. C **73**, 2636 (2013).
[67] V. Bertone, I. Scimemi, and A. Vladimirov, Extraction of unpolarized quark transverse momentum dependent parton distributions from Drell-Yan/Z-boson production, J. High Energy Phys. 06 (2019) 028.
[68] S. Tafat, Nonperturbative corrections to the Drell-Yan transverse momentum distribution, J. High Energy Phys. 05 (2001) 004.
[69] A. A. Vladimirov, Self-contained definition of the Collins-Soper kernel, Phys. Rev. Lett. **125**, 192002 (2020).
[70] F. Hautmann, I. Scimemi, and A. Vladimirov, Nonperturbative contributions to vector-boson transverse momentum spectra in hadronic collisions, Phys. Lett. B **806**, 135478 (2020).
[71] J. Collins and T. Rogers, Understanding the large-distance behavior of transverse-momentum-dependent parton densities and the Collins-Soper evolution kernel, Phys. Rev. D **91**, 074020 (2015).
[72] A. Vladimirov, Pion-induced Drell-Yan processes within TMD factorization, J. High Energy Phys. 10 (2019) 090.
[73] I. Scimemi and A. Vladimirov, Systematic analysis of double-scale evolution, J. High Energy Phys. 08 (2018) 003.
[74] M. Stratmann and W. Vogelsang, Next-to-leading order evolution of polarized and unpolarized fragmentation functions, Nucl. Phys. **B496**, 41 (1997).
[75] R. B. Wiringa, V. G. J. Stoks, and R. Schiavilla, An accurate nucleon-nucleon potential with charge independence breaking, Phys. Rev. C **51**, 38 (1995).
[76] J. L. Friar, B. F. Gibson, G. L. Payne, A. M. Bernstein, and T. E. Chupp, Neutron polarization in polarized ^{3}He targets, Phys. Rev. C **42**, 2310 (1990).